SAR AND TEMPERATURE ELEVATION IN SIX-LAYERED ADULT AND CHILD HEAD MODEL

by

Xintong Liu

A Thesis

Submitted to the Faculty of Purdue University

In Partial Fulfillment of the Requirements for the degree of

Master of Science in Electrical and Computer Engineering

Department of Electrical and Computer Engineering

Hammond, Indiana

May 2020

THE PURDUE UNIVERSITY GRADUATE SCHOOL
STATEMENT OF COMMITTEE APPROVAL

Dr. Khair A. Al Shamaileh, Chair

School of Electrical and Computer Engineering

Dr. Li-Zhe Tan

School of Electrical and Computer Engineering

Dr. Quamar Niyaz

School of Electrical and Computer Engineering

Approved by:

Dr. Xiaoli Yang

This thesis is dedicated to my family.

ACKNOWLEDGMENTS

I would like to show the highest respect to my advisor Prof. Khair Al Shamaileh. He is an enlightener on my research path. I really appreciate that he encourages and supports me constantly and always guides me in the right direction.

In addition, I would like to express my gratitude to my lovely family for supporting me to study abroad.

TABLE OF CONTENTS

LIST OF FIGURES

LIST OF TABLES

LIST OF SYMBOLS

P	Power (W)
H	Magnetic field intensity (A/m)
ρ	Density (kg/m^3)
σ	Conductivity (S/m)
E	Electric field (V/m)
C_o	Vacuum light speed (3× 10^8 m/s)
ε_r	Relative permittivity
ε_0	Vacuum permittivity (8.85×10^{-12}F/m)
G_m	Measured electrical conductance (S)
C_m	Measured capacitor value (F)
B	Magnetic field (T)
D	Electric displacement field(C/m^2)
μ	Permeability (H/m)
Δz	Dimensional step (m)
Δt	Time step (m)

ABSTRACT

With the development of wireless communication technology, second-, third-, fourth-generation transmission systems based on electromagnetic (EM) waves are widely used. At the same time, public concerns have been raised about whether the use of such systems will have an impact on health and safety standards. The heating effect is the most prominent and scientifically verifiable biological effect. So, the influence of EM waves on human body is addressed by studying the heating characteristics on head models.

The objective of this thesis is to study the effects of radio frequency (RF) waves radiation from mobile phones on the human head under different transmission generations. The six-layer head model is used to evaluate the specific absorption rate (SAR) distribution and thermal effect. This model allows to study the effects of SAR and temperature rise without the need for high computational resources. In order to find the effect of temperature rise and exposure time, the finite difference time domain (FDTD) method was used to solve the biothermal equation with appropriate boundary conditions.

Also, different age-dependent head models are used to study the differences of SAR for children at different ages.

In general, the results show that with the increase in frequency, the influence of the EM wave is more pronounced, as demonstrated by the SAR and temperature rise distribution. In addition, SAR distribution of younger ages show a significant increase, which indicates that children exposed to EM waves are subject to more harmed.

1. INTRODUCTION

1.1 Motivation

With the development of communication technology, the influence of mobile radiation has attracted a significant attention. Smartphones have been closely linked to human lifestyle; thus, the potential health hazards caused by the EM energy emitted by these devices require additional investigations.

Regulatory RF exposure bodies have been released in various countries, and SAR is used and standardized to describe the parameters of this effect. SAR parameters have been used widely to determine the possibility of RF radiation causing harm to human head. However, the biological effects of local SAR are still little known, and the physiologically based SAR distribution effects are unclear.

Since SAR refers to the EM radiation energy absorbed by a unit weight of material per unit time, which is a physical quantity used to measure the thermal effect of terminal radiation, so the safety criteria for wireless communication are determined based on the thermal effect of the head. In this thesis, the temperature rises in major layers (i.e., tissues) is mainly studied.

In light of the aforementioned discussion, in this thesis, the SAR of the human head for different ages will be determined considering planar multi-layered head models. In addition, due to emissions from wireless devices, the temperature rise in such models will be calculated by using the FDTD method to solve the biothermal equation under appropriate boundary conditions.

1.2 Basic Theory

1.2.1 EM Radiation

EM radiation is a phenomenon in which energy in the form of waves or particles travels in space. EM radiation describes an electric field and a magnetic field moving at the same time in space along the propagation direction. The basic unit of EM waves is photons. Higher frequencies are associated with higher photon energy.

Ionizing radiation and non-ionizing radiation are two types of EM. Ionization refers to the process where electrons are escaping from atoms and molecules. This process causes the variation of molecular that cause damage to biological tissues, including genetic material DNA. Ionizing

radiation requires high-energy photon interactions; while RF radiation, including radio waves and microwaves, is a different form of energy. The frequency range of an RF waves is 3 kHz to 300 GHz, and the energy of photon will not let atoms and molecules be ionized. Therefore, RF radiation and some other forms of low frequency electrical radiation are collectively referred to as "non-ionizing radiation" [1].

Biologically speaking, the effects of RF radiation that results in tissue heating are generally referred to as "thermal effects". It has been identified long time ago that RF can heat biological tissues as the human body cannot handle the excessive external heat generate. Exposed to an RF field with a power density of 1-10 mW / cm^2 may generate heat in biological tissue under certain conditions, but these thermal effects are very small and are not sufficient to cause damage. The frequency of radiation, the size, shape, polarization direction of the radiated object, the length of radiation time, the surrounding environmental conditions and the heat dissipation rate will cause different thermal effects [2].

Studies in bioelectromagnetic have shown that the human eye [3], for example, is one of the most vulnerable tissues to thermal effects as it lacks effective blood circulation to dissipate excess heat. Biological experiments have shown that high-power RF radiation (100-200mW/cm^2) can cause cataract in rabbits in a short period of time. In real life, RF power that ordinary people are exposed to is generally safer, but in some special working environments close to high-power RF sources, the RF intensity may exceed the safety limit for human radiation, so that strict measures should be taken to ensure the safety of the human body.

1.2.2 Specific Absorption Rate (SAR)

For decades of years, the general public has been concerned about the potential health effects of RF radiation on the human body. During a call, cell phone radiation can raise the temperature of the human head by few degrees Celsius.

At the operating frequencies of most of these mobile communication devices, the known effects of radiation exposure are based on the thermal effect of human tissue, which generates an induced EM field under the action of an external one. Since all kinds of organs in the human body are lossy media, the EM field in the body will generate electric current that causes absorption and dissipation of energy. This heating physical process is commonly used in biological dosimetry.

SAR is the EM wave absorption ratio. It is the ratio of EM wave energy absorption of mobile phones or wireless products. It is a numerical description of the induced EM field in a human body under the action of external EM field. The expression of SAR shows as follows:

$$\text{SAR} = \frac{P}{\rho} = \frac{\sigma\frac{\boldsymbol{E}^2}{2}}{\rho} = \frac{\sigma \boldsymbol{E}^2}{2\rho} \tag{1.1}$$

where σ is conductivity (S/m), P is power, $\boldsymbol{E}$ is the electric field strength, and ρ is the tissue density.

1.3 The Harm of Mobile Phone Radiation to the Human Body

Radiation is a result of the propagation of EM waves. For example, mobile phone radiation is generated when a mobile phone sends radio waves to a base station while being used.

There are two ways of radiation harm to the human body: “non-thermal effect” and “thermal effect”. The non-thermal effect is that when weak microwave energy is radiated into the human body, potentially causing a series of abnormal symptoms Laboratory studies have shown that microwaves can change the arrangement of their own polar molecules and the movement of free charges and ions, affecting the formation of free radicals and leading to oxidation of proteins, DNA breaks, and grid apoptosis [4]. As a result, people with neurological disorders, behavioral disorders, irritability, headaches, memory loss and other phenomena are the most vulnerable to this harmful effect. A thesis on cell phone carcinogenesis in the internationally scientific journal “Variation” puts forward the theory that “cell phone radiation generates heat shock; protein destroys grid defense system to cause cancer” and establishes scientific evidence for cell phone radiation carcinogenesis [5].

1.4 EM Regulations and SAR Standard

Cell phone radiation has long received public attention. Different countries have different regulations on mobile phone radiation safety standards. The most widely used safety guideline is given by International Commission on Non-Ionizing Radiation Protection (ICNIRP). American National Standard Institution and Institution of Electrical and Electronic Engineering (ANSI&IEEE) has developed the standard used in the U.S. [6-7] Both of these two standards are

derived from the results of animal experiments. As a result, sets of maximum tolerable values of SAR have been proposed.

Table 1.1 Limits and measurement methods for SAR in the world

Country	Standard	Whole Body (W/kg)	Peak (W/kg)	Average Time (min)	Average Weight (g)
Australia	AS2772.1/ARPANSA	0.08	2	6	10
New Zealand	NZS2772.1	0.08	2	6	10
USA	ANSI C95.1	0.08	1.6	30	1
Europe	EN50360	0.08	2	6	10
Japan	TTC/MPT	0.08	2	6	10
Taiwan	DGT	0.08	1.6	30	1
International	ICNIRP	0.08	2	6	10

In this thesis, dosimetry is introduced to predict the electromagnetic field dose at any point inside or outside the human body. Dosimetry can determine the amount of power, electric field and current that appear in various parts of body due to different electric field exposures. When formulating rules, you need to understand whether the physiological reactions caused by electromagnetic radiation are harmful to the human body, so that these effects or reactions are used to define the allowable criteria or regulations for electromagnetic field exposure. In addition, the guidelines usually specify the allowable exposure intensity and allowable frequency.

All guidelines are developed for safety limits for time-varying EM, magnetic and electric fields. These guidelines apply to electromagnetic exposure by the general public. ICNIRP limits are the restrictions, which are directly based on recognized effects on health that are exposed to time-varying fields. Individual reference limits are based on the sensation and adverse indirect effects of human exposure to EM fields.

From February 1, 1999, Europe implementing the mobile phone EM radiation protection standard IEEE1528SAR-200X, which was regulated by ICNIRP for mobile devices [6]. The limit of SAR was set to 2 W/kg over 10 g. This standard has been adopted and accepted by most countries and regions in the world. According to research on animals, 4 W/kg has been recognized as the upper limit of exposure of the entire organism to RF. For the general public, the 2 W/kg exposure limits established by the ICNIRP have left a large margin of safety. Because this standard is based on careful analysis of all scientific data and provides significant safety assurance for all

identified RF radiation hazards, it is supported and adopted by the world health organization (WHO) and is also recommended by international telecommunication union (ITU). Looking back at the United States in 1997, the Federal Communications Commission (FCC) required the SAR of phones sold to be equal to or lower than 1.6 watts per kilogram (W / kg), which is based on the energy absorbed by 1g of tissue. Table 1.1 shows the limits and measurement methods for SAR in major countries and regions of the world.

1.5 Thesis Scope

In this thesis, the FDTD method is used to study the influence of RF radiation of mobile devices on the human head in different transmission generations. The use of a seven-layer head model makes it more efficient to study the effects of temperature rise and SAR distribution in multiple tissue types. In addition, a child head model will also be used to evaluate SAR distribution based on age. In this thesis, the biothermal equation with appropriate boundary conditions is calculated by FDTD method to evaluate the temperature rise in head tissues as a function of RF exposure time.

2. LITERATURE SURVEY

In 1996, Niels and Kuster[8] of the Swiss federal institute of technology (FIT) first developed the EM radiation dose evaluation device in the world, which was used to test the SAR and the near-field electric and magnetic fields. The device mainly includes a measurement part, control part and human body model. The measuring part is composed of a probe, an optical fiber, and a data acquisition system. The control part is composed of an industrial robot, an insulating board, and a surface detector robot controller. This device is widely used in research and development in Japan, Europe, and the US.

In 2002, Neubauer made the comparison of the EM radiation between the human head and the mobile phone antenna at operating frequencies of 433MHz, 900MHz, 1300MHz, 1800MHz and 2450MHz [9].

In 2003, Fang simulated the impedance characteristics, far-field radiation characteristics, internal electric field distribution, and current distribution, to model the radiation effects on the human body considering dual-frequency PIFA [10]. In 2003, Xiaoming used a three-layer spherical head model to emulate and calculate SAR under the action of a monopole antenna using the FDTD method at a frequency of 900MHz [11].

In 2004, Choi1, Shin began to analyze the mechanism of the EM radiation of the mobile communication terminal on the human body [12]. By using the FDTD method, the SAR value distribution was established. Curves and three-dimensional distribution diagrams were used to analyze the absorption of radiation from mobile communication terminals in the human body, and a direct and effective method for reducing SAR values was proposed.

In 2009, Oskooi et al. Of the MIT developed MEEP [13], which is the most widely used electromagnetic radiation simulation software based on the FDTD algorithm. Dispersive materials, PML absorption boundaries, periodic boundaries, etc., can be accelerated in parallel by distributed memory CPU. By improving grid division, spatial coordinate system and absorption boundary conditions, MEEP can be very convenient and fast for targets with symmetric structures Calculation, and has the functions of calculating the flux of the specified surface, analyzing the resonance mode, frequency domain analysis and so on.

In 2009, Sabbah and Dib used FDTD method to develop the SAR and temperature rise assessment of a multi-layered human head model that was exposed to radiation caused by telephones and WLAN antennas [14].

In 2013, Çapoğlu and Taflove of Northwestern University developed Angora software based on FDTD algorithm [15], which can perform CPU parallel acceleration calculation based on MPI parallel standard, support complex beam wave source, use CPML technology as absorption boundary, support dispersive materials, and provide Optical image simulation function.

In 2017, Mohammed and Jin evaluated children exposure to EM fields with 3D child head model [16]. The 3D models are real MRI model from volunteers, and the dielectric properties of biological materials were generated by age. It compared the SAR of different age head model under various conditions,

3. NUMERICAL METHOD AND MODELLING

3.1 Adult Head Model and Properties

A planar six-layered human head model, which was proposed by Abdalla and Teoh in 2005 has been used as a head model, where the CSF is cerebrospinal fluid, and the brain includes grey matter and white matter. As shown in Figure 2.1, the thickness of the skin is 0.07cm, fat is 0.16cm, bone is 2.05cm, dura is 0.05cm, CSF is 0.2 cm, and brain is infinite [17].

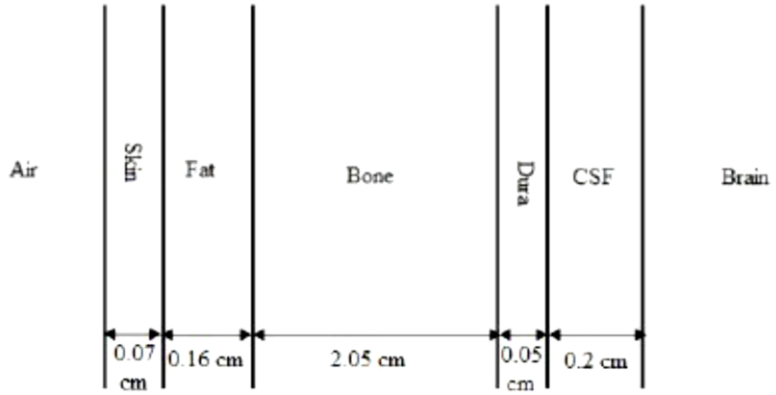

Figure 3.1 Planar six-layered adult human head model [17]

Due to the small number of existing anatomical models and the inability to give accurate material proportions, this work will use a planar six-layer model to study SAR effects, considering to different ages.

The human body's field is a combination of biological electromagnetic fields. The relative permittivity, ε_r,and the conductivity, σ, are two key parameters for modeling electrical properties including the attenuation of EM waves and current conduction.

Table 3.1 presents density of each layer in an adult head model. All of these tissue density values are so stable that will not be changed with temperature, frequency, or age.

Table 3.1 Material density of an adult human head [18]

Material	Bone	Skin	CSF	Dura	Brain	Fat
$\boldsymbol{\rho}$ (10^3kg/m^3)	1.85	1.1	1.06	1.05	1.03	0.92

Table 3.2 Relative permittivity of different tissues in an adult human head

Freq / Layer	Relative permittivity ε_r at different frequencies (MHz)							
	700	**850**	**900**	**1800**	**2100**	**2300**	**2400**	**2600**
Skin	42.698	41.68	41.4	38.9	38.43	38.179	38.1	37.85
Fat	5.497	5.47	5.46	5.34	5.32	5.3	5.29	5.26
Bone	12.66	12.5	12.45	11.8	11.59	11.47	11.41	11.29
Dura	44.996	44.55	44.4	42.9	42.49	42.23	42.1	41.84
CSF	69.16	68.75	68.7	67.2	66.76	66.47	66.3	66.02
Brain	46.797	46.02	45.8	43.5	43.06	42.75	42.6	42.33

Table 3.3 Conductivity of different tissues in an adult human head

Freq / Layer	Conductivity(S/m) σ at different frequencies (MHz)							
	700	**850**	**900**	**1800**	**2100**	**2300**	**2400**	**2600**
Skin	0.79996	0.85	0.87	1.18	1.31	1.395	1.44	1.54
Fat	0.047	0.05	0.051	0.078	0.0899	0.098	0.102	0.11
Bone	0.12	0.14	0.14	0.28	0.33	0.37	0.385	0.42
Dura	0.902	0.95	0.96	1.32	1.47	1.58	1.64	1.76
CSF	2.34	2.39	2.41	2.92	3.15	3.32	3.41	3.6
Brain	0.695	0.75	0.77	1.15	1.31	1.42	1.48	3.2

Tables 3.2 and 3.3 [19] show ε_r and σ of each material in the adult head model at 2-G (i.e., 700 MHz, 850 MHz, 900 MHz), 3-G (i.e., 1800 MHz, 2100 MHz,), and 4-G (i.e., 2300 MHz,2600 MHz) frequencies. In principle, the dielectric properties (4-Cole-Cole model) of a sample are calculated by the following relationship: [4]

$$\sigma = \frac{G_m \varepsilon_0}{[(1+\omega^2 LC_m)^2+(\omega LC_m)^2]K} \tag{3.1}$$

$$\varepsilon(\omega) = \varepsilon_\infty + \sum_{m=1}^{4} \frac{\Delta\varepsilon_m}{1+(j\omega\tau_m)^{1-a_m}} + \frac{\sigma_j}{j\omega\varepsilon_0} \tag{3.2}$$

ε_0 is the permittivity of vacuum (8.85×10^{-12}F/m), ε_∞ is the dielectric constant in the range of terahertz frequency, τ_m is relaxation time, $\omega = 2\pi f$, $L = 2 \times 10^{-7} H$, G_m and C_m are the measured capacitance and conductance, sum of 4 is 4-Cole-Cole model. With the increase in frequency, ε_r decreases; whereas σ increases.

3.2 Electrical Power Density

In bio electromagnetism, when the materials are different, the EM field changes accordingly, and this change also reflects the different effects on human bodies. Since the electric and the magnetic fields are the forces of charge and charge interaction, the interaction between fields and the material is the force to which the material is subjected.

The concept of conductivity is introduced because biomaterials are lossy. Since the energy transfer in the electric field is mainly transferred to the electric charge, and the electric charge in the magnetic field cannot receive the energy propagation, the interaction between the EM field and the material will ignore the effect in magnetic field. Therefore, in a steady-state EM field, the electric power density appears as [20]

$$P = \sigma \frac{\boldsymbol{E}^2}{2} (W/m^3) \tag{3.3}$$

3.3 Numerical Calculation Methods

The ultimate requirement for solving EM field problems is to find an exact or a closed form analytical solution to Maxwell's propagation equations under given and support it with a physical interpretation. In modern EM field engineering, it is very challenging and cumbersome to obtain analytical solutions. Even a semi-analytical approximation method can only be used in a limited number of applications. Rather, the widely used methods are based on numerical analysis. (e.g., FDTD, transmission line matrix method, time domain integral equations). In addition, there are geometric diffraction theories to solve high frequency propagation. Each method has its own characteristics and limitations. In practice, methods often are used in parallel to form various combinations.

3.3.1 **Direct Frequency Domain**

Direct frequency domain methods can be divided into integral equation forms and differential equation forms. The form of the integral equation is to treat the action of the EM field as a boundary value problem. According to the boundary condition, an integral equation or an integral differential equation is derived for the electric field or the magnetic field. However, these equations are not general and require re-derivation for specific geometric boundaries and material properties. The moment method is the most widely used approximation method for solving such integral equations. First, the integral equation is converted into an equivalent matrix equation, and then the matrix equation is inversely calculated. This method is versatile and can be applied to any shape and non-uniformity problem. However, it may result in very large matrices and can lead to ill-conditioned matrices that limit their use. Recently, iterative techniques such as the fast Fourier transform and conjugate gradient method have been used, which has extended the application range of the moment method.

The differential form method is mainly the finite difference method and the finite element method. The finite element method requires a variational form of the differential equation, but it is not valid for all problems. The main disadvantage of these two methods is that they require more storage space and computation time. In the form of differential equations, there is also a single moment method. The main point of this method is to surround a given structure with a spherical or cylindrical surface according to the dimension of the problem. The minimum radius is chosen to enclose the structure in order to make the outer region the scattering field can be represented by an external ball or column function, and the finite element method can be used to solve the Helmholtz equation in the inner region. This method maintains the advantages of the finite element method.

3.3.2 **Direct Time Domain**

The direct time domain method can also be divided into two forms: integral equations and differential equations. The integral equation form is generally called the hysteresis bit integration method. This method uses the Green function and the boundary conditions of the scattered surface to establish the time domain integral equation. The basic method of solving the equation is to discretize the integral region and the time variable of the spatial variable, and then transform the integral equation into a linear system of equations. Different from the direct frequency domain

method, the equations are not solved by the inverse matrix method but based on the following considerations. When the applied excitation does not reach the reflector, the induced current is zero everywhere, because the propagation velocity of the field is Limited, the values of the points in the space before the influence of the excitation have not reached before the field value is zero. Moreover, the response of a point in space at a certain moment is only affected by the excitation source that satisfies the hysteresis relationship. This is calculated from the initial value, and the field value of each time sampling point is obtained by time stepping. The main advantage of this method is that the computational area is limited to the surface of the structure. The disadvantage is that it requires post-time storage to complete the deferred integration and increase the storage space requirements.

The main use of the differential form is the FDTD method. This is a method of maintaining the time variable in the Maxwell's curl equation, which is solved directly in the time and space without transformation. It can provide all solutions to the homogeneous part (instantaneous) and non-homogeneous part (steady state) of the equation. It repeatedly runs the finite difference format directly converted from the Maxwell curl equation in each grid, thereby simulating the propagation of electromagnetic waves and the action of objects by computer. Post-storage is not required in this simulation, and generally only involves field values at the previous point in time. A disadvantage of this method is that the calculation area must not only be on the surface of the structure but must also include the interior and enough external space to effectively satisfy the radiation conditions. However, since it uses the most common Maxwell equation as a starting point, it has a very wide range of applications.

3.3.3 **High Frequency Approximation**

For a large electric object, if the medium characteristics and geometric parameters are slowly changing, the propagation of the electromagnetic wave has a local property, that is, the electromagnetic field of a given observation point depends only on the distribution of the electromagnetic field on a limited area of the curved surface. In this case, the calculation of the electromagnetic field can use a so-called high frequency approximation, which mainly refers to the geometric theory of diffraction (GTD).

The GTD is derived from geometry in which diffracted rays are introduced to eliminate the discontinuity of the field at the boundary of the geometrical optical ray and in the region between

these boundaries, especially in the zero-field region expected by geometric optics. Introduce the appropriate field for correction. According to the local field principle, the GTD method decomposes objects into some typical geometric configurations, and then performs field calculation based on the diffraction fields of these typical geometric structures. The GTD method has been proven to be useful for solving many large electrical problems, but in the transition zone near the shadow boundary and near the reflection boundary, and in the defocusing direction expected to be an infinite field along the GTD formula, the nature of the illumination field is complex. These field GTD methods are not applicable. In order to overcome the above difficulties, a uniform diffraction theory, a consistent progressive theory, a physics theory of diffraction, and a spectral theory of diffraction were developed.

3.3.4 Comparison of Methods

The high frequency approximation method is suitable for calculating the EM field problem of electrically large conductors, but it is difficult for systems composed of small electrical conductors and media or other non-metallic materials. The opposite moment method and FDTD method are suitable for applications near low frequency or resonant frequency and can be used for near-field and far-field calculations and can be applied to systems composed of metal and dielectric materials. The FDTD method not only has stronger ability to simulate various complex structures, but also avoids solving equations, so it has a stronger ability to simulate various complex structures. The storage space and calculation time required by FDTD are only related to Number of cells in grid space, N.

3.4 The Finite-Difference-Time-Domain (FDTD) Method

Computational electromagnetics are used calculate the interaction between the field and the medium in an uneven material. In this thesis, FDTD [21-28] is used, since it can directly simulate the distribution of the field, and the accuracy is relatively high.

The finite-difference time-domain method uses the finite-difference formula to replace the differential expression in the time-domain field curl of Maxwell's equations, to obtain the differential equations about the field components. The initial value and the boundary conditions of the calculation space can obtain the four-dimensional numerical solution of Maxwell's equations including time variables.

The time-domain finite difference method has great advantages. First, the storage space and calculation time required by the algorithm is only proportional to the number of cells in the grid space, so a more accurate non-uniform block model of the human body can be used, which greatly improves the calculation accuracy and provides richer information. Secondly, the time-domain finite difference method can automatically meet the discontinuous boundary conditions, avoiding the calculation errors that other methods may generate on this boundary, which also makes it easier to build the human body model, and it can still maintain a good convergence characteristic. Third, the finite-difference time-domain method can easily simulate the radiation structure and its radiation characteristics, so that the interaction between the radiation near field and the human body model can be simulated in the same grid space. Finally, when it is necessary to understand the effect of the pulse field on the human body, the time-domain finite difference method needs only one operation to obtain all the information. This is the characteristic of the time-domain method.

As the moment method of frequency domain method, it can only take Fourier transform to the pulse, and then calculate each frequency spectrum. If you need to understand the time domain characteristics, you must also inverse Fourier transform the calculation results of all the spectrum. Of course, because the human body is a dispersive medium, when calculating the effect of the pulse on the human body, the improved finite difference method in the time domain must be used.

In order to introduce the basic principles of FDTD, the characteristics of Maxwell's equations in linear media need to be analyzed. Maxwell's equations in linear media are expressed in Equation 3.4.1-3.4.4 as follows:

$$\nabla \times \boldsymbol{E} = -\frac{\partial \boldsymbol{B}}{\partial t} \tag{3.4.1}$$

$$\nabla \times \boldsymbol{H} = -\frac{\partial \boldsymbol{D}}{\partial t} + J \tag{3.4.2}$$

$$\nabla \cdot \boldsymbol{D} = \rho \tag{3.4.3}$$

$$\nabla \cdot \boldsymbol{B} = 0 \tag{3.4.4}$$

where the $\boldsymbol{B}$ is magnetic flux density (Wb/m^2), $\boldsymbol{H}$ is magnetic field strength (A/m), ρ is charge density (C/m^3), and $\boldsymbol{D}$ is Electric displacement vector (C/m^2). The relationship between them show as following:

$$\boldsymbol{B} = \mu \boldsymbol{H} \tag{3.4.5}$$

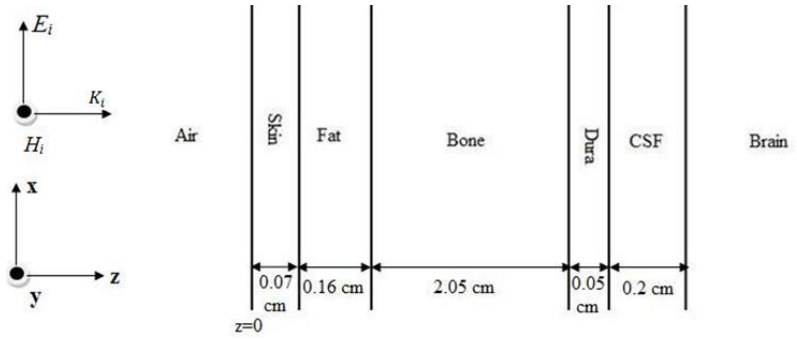

Figure 3.2 A normal plane incident wave of an adult human head model

$$\boldsymbol{D} = \xi \boldsymbol{E} \tag{3.4.6}$$

In a homogeneous isotropic medium, μ and ξ are scalar constants. For non-uniform isotropic media, μ and ξ are scalar that varies with spatial location. For anisotropic media, μ and ξ are tensor.

Usually at the beginning, both the field and the source are set. At this time, the two divergence equations will be included in the two curl equations and the initial boundary conditions, which are redundant. The FDTD formula only requires the curl of Maxwell's equations. Therefore, considering the material permeability μ, permittivity ε, and electric conductivity σ, the Maxwell curl equations for linear, isotropic, source-free media are given as:

$$\nabla \times \boldsymbol{H} = \sigma \boldsymbol{E} + \varepsilon \frac{\partial \boldsymbol{E}}{\partial t} \tag{3.5}$$

$$\nabla \times \boldsymbol{E} = -\mu \frac{\partial \boldsymbol{H}}{\partial t} \tag{3.6}$$

For 1-D case, the polarization direction of the electric field is x, the polarization direction of the magnetic field is y, and the direction of propagation is z. All physical quantities are constant in the x, y plane, but only a function of z, the Maxwell's equations become:

$$\frac{\partial \boldsymbol{E_x}}{\partial z} = -\mu \frac{\partial \boldsymbol{H_y}}{\partial t} \tag{3.7}$$

$$\frac{\partial \boldsymbol{H_y}}{\partial t} = -\varepsilon \frac{\partial \boldsymbol{E_x}}{\partial t} \tag{3.8}$$

According to the Figure 3.2, the incident plane wave on the interface of an adult head model in free space is presented by electric field intensity, $\boldsymbol{E}_i$, magnetic field intensity, $\boldsymbol{H}_i$, and propagation vector, $\boldsymbol{k}_i$. Because it is a normal incident wave, $\boldsymbol{k}_i$ is perpendicular to the model

interface, which makes the $\boldsymbol{E}_i$and $\boldsymbol{H}_i$vectors tangent to the surface. Therefore, the Maxwell curl equations of a plane wave change to:

$$\frac{\partial \boldsymbol{E}_x}{\partial t} = -\frac{1}{\varepsilon_0 \varepsilon_r}\frac{\partial \boldsymbol{H}_Y}{\partial z} - \frac{\sigma}{\varepsilon_0 \varepsilon_r}\boldsymbol{E}_x \tag{3.9}$$

$$\frac{\partial \boldsymbol{H}_y}{\partial t} = -\frac{1}{\mu}\frac{\partial \boldsymbol{E}_x}{\partial z} \tag{3.10}$$

which shows the plane wave only has an electric field in the x direction and a magnetic field in the y direction, and both travelling in the z-direction.

In FDTD, space is divided into multiple units. In other words, $\boldsymbol{E}$ and $\boldsymbol{H}$ should be determined at discrete spatial locations. In this case, $\boldsymbol{E}$ and $\boldsymbol{H}$ are staggered, as represented in Figure 3.3.

According to Figure 3.3, the magnetic field strength $\boldsymbol{H}_y(t-\frac{1}{2}\Delta t)$ is updated by electric field strength $\boldsymbol{E}_x(t-\Delta t)$ and $\boldsymbol{E}_x(t)$. Then, another new electric field strength $\boldsymbol{E}$ will be generated by the $\boldsymbol{H}_y(t-\frac{1}{2}\Delta t)$ and $\boldsymbol{H}_y(t+\frac{1}{2}\Delta t)$.

Table 3.4 shows the math procedure of FDTD method, which represents the way of updating $\boldsymbol{E}$ and $\boldsymbol{H}$. Δt shows in the procedure is time step.

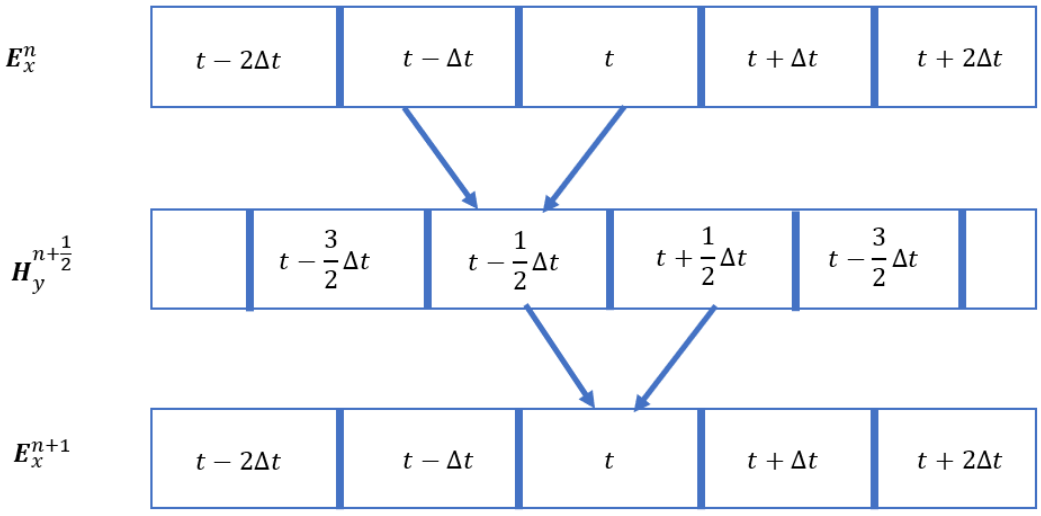

Figure 3.3 Staggered distribution of $\boldsymbol{E}$ and $\boldsymbol{H}$ fields in space-time in FDTD method

The pseudo code (Algorithm 1) is the main loop of FDTD method that represent the math procedure of FDTD method in Table 3.4.

Table 3.4 Math procedure of FDTD method

$\nabla \times \boldsymbol{E} = -\mu \frac{\partial \boldsymbol{H}}{\partial t}$	**Maxwell's Equations**	$\nabla \times \boldsymbol{H} = \varepsilon \frac{\partial \boldsymbol{E}}{\partial \mathrm{t}}$
$\frac{\partial \boldsymbol{H}}{\partial t} = -\frac{1}{\mu} \nabla \times \boldsymbol{E}$	**Rearrange**	$\frac{\partial \boldsymbol{E}}{\partial \mathrm{t}} = \frac{1}{\varepsilon} \nabla \times \boldsymbol{H}$
$\frac{\boldsymbol{H}\left(t+\frac{\Delta t}{2}\right) - \boldsymbol{H}(t-\frac{\Delta t}{2})}{\Delta t} = -\frac{1}{\mu} \nabla \times \boldsymbol{E}(t)$	**Finite Difference Approximation**	$\frac{\boldsymbol{E}(t+\Delta t) - \boldsymbol{E}(t)}{\Delta t} = \frac{1}{\varepsilon} \nabla \times \boldsymbol{H}(t+\frac{\Delta t}{2})$
$\boldsymbol{H}\left(t+\frac{\Delta t}{2}\right) = \boldsymbol{H}(t-\frac{\Delta t}{2}) - \frac{\Delta t}{\mu} \nabla \times \boldsymbol{E}(t)$	**Update $\boldsymbol{H}$ and $\boldsymbol{E}$**	$\boldsymbol{E}(t+\Delta t) = \boldsymbol{E}(t) + \frac{\Delta t}{\varepsilon} \nabla \times \boldsymbol{H}(t+\frac{\Delta t}{2})$

Algorithm 1. FDTD

Given: [σ] - Tissue conductivity

[k] - Number of cells.

[f] - Frequency

[N] -Step of frequency

[st] - Number of time steps

Procedure: FDTD ()

```
for t = 1 : st
    % Update E from H
        E(k) ←H(k-1/2) + H(k+1/2)
    % Record E-Field at Boundary
        E(k)←Ex(k)
    % Update H from E
        H(k+1/2) ← E(k)+ E(k+1)
    % Record H-Field Boundary
        H(k+1/2) ←Hy(k+1/2)
    % Update Fourier Transforms
        for x = 1: N
            Calculate SAR, T
        end
      % Print out result
        Plot SAR, T
end
```

3.4.1 **Cell Size Determination**

The method of how to choose the cell size in the FDTD is as follows: the sampling point must be enough to ensure enough representation. Through literature search, 10 cells per wavelength is sufficient to avoid errors.

For instance, suppose that the frequency is 850 MHz. In free space, the propagation wavelength is:

$$\lambda = \frac{C_0}{f} = \frac{3\times10^8}{850\times10^6} = 0.353\ m \tag{3.11}$$

where $C_0$is the light speed in free space. Therefore, the dimensional step should satisfy:

$$\Delta z \leq \frac{\lambda}{10} = 3.523\ cm \tag{3.12}$$

Additionally, since the tissue thicknesses of the head are such thin, a sufficiently small step size to represent all tissues need to be selected. Therefore, the cell size is set to 0.1 mm.

3.4.2 **Numerical Stability Analysis**

FDTD is a differential algorithm, so the time step, Δt and space step should follow certain rules, otherwise stability problems will occur. In other words, the resulting instability is not due to the accumulation of errors, but due to the artificial causality between the time and space steps that destroys the propagation of electromagnetic waves.

When comparing the variation range of the time eigenvalue and the space eigenvalue, the actual situation should be considered. Both the time and space eigenvalues should be meaningful and should fall within the required values and eigenvalue spectrum. Therefore, if it is required to meet the numerical requirements of both time and space eigenvalues, the following equation must be satisfied:

$$\Delta t \leq \frac{1}{v\sqrt{\frac{1}{(\Delta x)^2}+\frac{1}{(\Delta y)^2}}} \tag{3.13}$$

Equation 3.13 is also called Courant stability condition.

In free space, since the propagation speed of EM waves cannot exceed the light speed, when the speed is the same as C_0, the minimum Δt required to propagate the distance of a cell can be obtained.

In this thesis. Δt which achieves the Courant stability condition is chosen such then:

$$\Delta t = \frac{\Delta z}{2C_0} \tag{3.14}$$

The algorithm 2 shows the pseudo code of finding the time step size to make the result stable.

Algorithm 2. Time Step Stability Criterion

Given: [$freq\_in$] - Frequency

[C_0] - Light speed in free space

Procedure:

```
% Compute wavelength
lambda=C0/(freq_in);
% Compute cell size
ddx = lambda/10;
% Calculate the time step size
dt = ddx/(2*C0);
```

3.4.3 Absorption Boundary Condition

The FDTD algorithm must set the absorbing boundary condition for calculating the space boundary. When FDTD is used to analyze the open or semi-open nature of EM radiation and scattering, it is difficult to directly calculate infinite structures. Therefore, appropriate absorption boundary conditions should be set at the truncation to simulate the infinite length transmission structure of open infinite space or finite grid space. The ideal absorption boundary condition is that on the truncated boundary there are only outward waves and no inward waves.

Usually, the guided wave system is assumed to be infinitely long. When the EM field problem is solved by the FDTD method, the space is assumed to be infinite or so-called “open” system. The six field components on each cell grid need to be stored and provided to the next time unit to continue calculations. Therefore, the larger the space for the problem being studied, the greater the amount of storage required. When modeling, in order to make the limited space become like an infinite space, the surrounding boundary of the limited space needs special treatment, then the following conditions should be satisfied: First, the wave traveling to the edge interface keeps the "outward travel"; Second, it will not cause reflection; Third, the field in the internal space will not be distorted. Boundary conditions can meet the above description is absorbing boundary conditions.

According to [22], the value on one side of the edge of the problem space is not available, and there is no source outside it. Therefore, the field at the borderline must propagate outwards, so that the value will be estimated by the value near it.

Since this is a planar model, only the boundary problem on the plane needs to be considered. Moreover, both $\boldsymbol{E}$ and $\boldsymbol{H}$ propagate in one direction, so only the boundary conditions at the beginning and the end need to be considered. The boundary condition of the beginning and the end shows in Equation 3.15-3.18.

1. At the beginning of the head model:

   In free space, suppose that a wave is going toward a boundary, which is traveling at C_0, the speed of light. So, the distance it travels in one Δt of the FDTD is equal to:

$$\mathrm{D} = C_0 \Delta t = C_0 \frac{\Delta z}{2C_0} = \frac{\Delta z}{2} \tag{3.15}$$

   Boundary condition:

$$\boldsymbol{E}_x^n(0) = \boldsymbol{E}_x^{n-2}(1) \tag{3.16}$$

   Therefore, the value of $\boldsymbol{E}_x\,(1)$ is stored for 2 time steps, and then used in $\boldsymbol{E}_x\,(0)$.

2. At the right end of head model:

   For the end of head model, the ε_r of the last layer, which is brain, have to be taken into account.

$$\mathrm{D} = V\Delta t = \frac{C_0}{\sqrt{\varepsilon_r}} \frac{\Delta z}{2C_0} = \frac{\Delta z}{2\sqrt{\varepsilon_r}} \cong \frac{\Delta z}{S} \tag{3.17}$$

   Boundary condition:

$$\boldsymbol{E}_x^n(KE) = \boldsymbol{E}_x^{n-S}(KE-1) \tag{3.18}$$

where *n* is the number of dimensions, $S \geq 2$ since the wave takes at least two steps to cross a nearby cell, and *KE* is the last cell in the model.

3.4.4 Excitation Source

Broadly speaking, excitation sources are usually of two types: sinusoidal signal excitation sources and Gaussian pulse excitation sources. Through experimental comparisons, it is found that these two sources give the same results at the same frequency. In this thesis, Gaussian pulse excitation sources will be used.

In theory, the results of various frequency ranges can be obtained with only one simulation. However, for human SAR calculations, the wide frequency range has limited practical benefits

because human tissue parameters depend on frequency, which would be a large computational burden. Therefore, the results from the Gaussian excitation are correct only at a single frequency that defines the tissue parameters. For pulse excitation, the method used can be divided into three steps:

1. Find Gaussian pulse excitation sources expression.
2. Record the $\boldsymbol{E}$ and $\boldsymbol{H}$ required for each Δt
3. Calculate discrete Fourier transform.

The Gaussian pulse excitation sources expression is as follow:

$$\boldsymbol{E}_x = \boldsymbol{E}_0 e^{-[\frac{(n-n_0)}{n_{decay}}]^2} \tag{3.19}$$

where n_{decay} is the Gaussian pulse standard deviation, and the center of pulse n_0 is:

$$n_0 \geq 3n_{decay} \tag{3.20}$$

The maximum frequency is

$$f_{max} = \frac{1}{2\,\Delta t\, n_{decay}} \tag{3.21}$$

Fourier transform shows as:

$$E = \sum_1^{NSteps} \boldsymbol{E}^n e^{-j2\pi f\, n\, \Delta t} \tag{3.22}$$

The amplitude is chosen as 300 V/m, since it's the highest level a mobile phone may cause [29-31]. In order to achieve 300V/m in 2-G,3-G,4-G frequency, $\boldsymbol{E}_0$, and n_0 should be chosen as follows:

1. Frequency=700MHz, $E_0 = 1.48$, $n_0 = 120$,$n_{decay} = 400$, $A = 300\,V/m$.

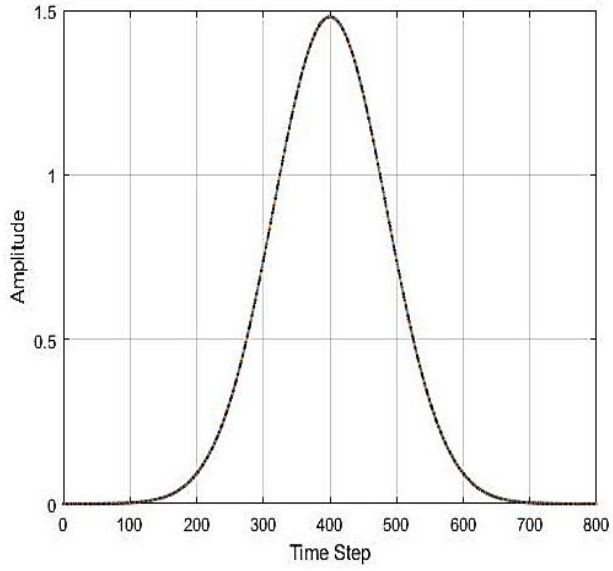

Figure 3.4 Time-domain Gaussian pulse at 700MHz

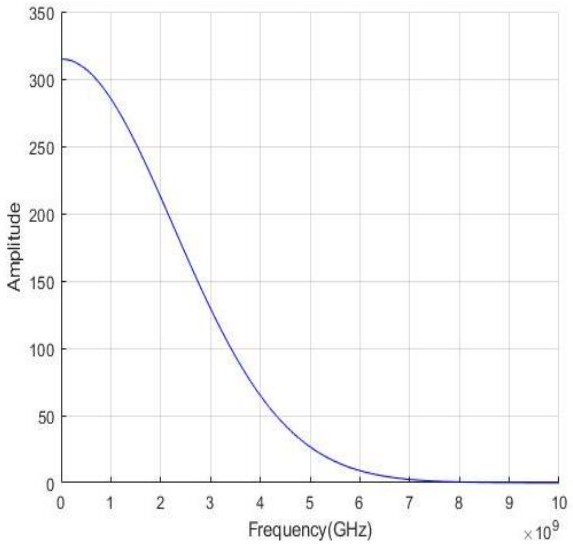

Figure 3.5 Fourier transform of 700MHz Gaussian pulse

2. Frequency=850MHz, $E_0 = 1.515$, $n_0 = 120$,$n_{decay} = 400$, $A = 300\,V/m$.

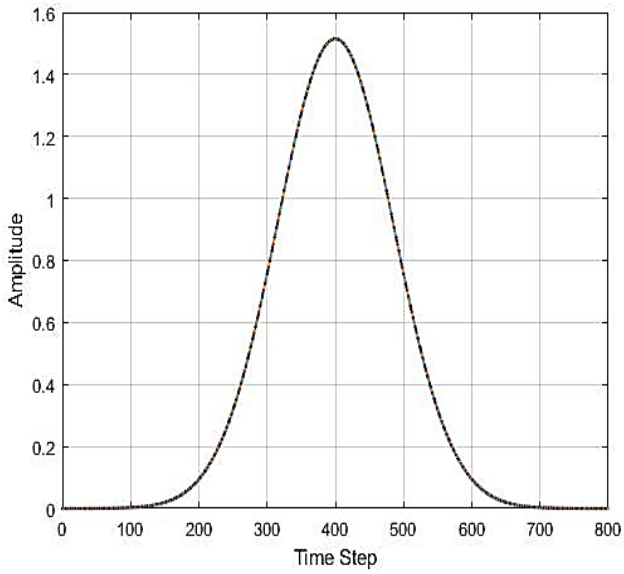

Figure 3.6 Time-domain Gaussian pulse at 850MHz

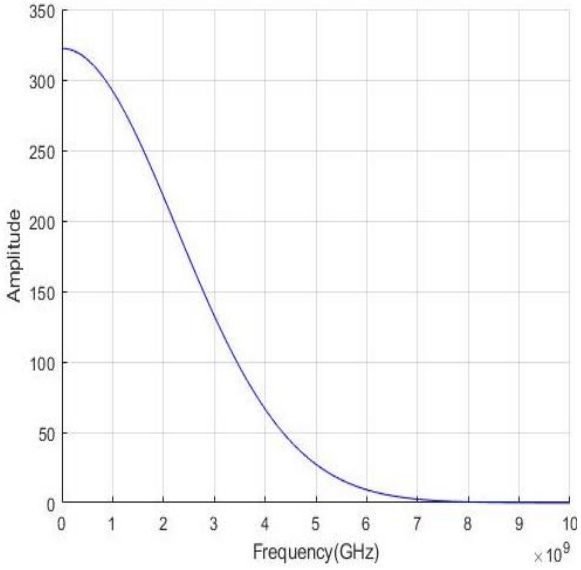

Figure 3.7 Fourier transform of 850MHz Gaussian pulse

3. Frequency=2100MHz, $E_0 = 2.18$, $n_0 = 120$,$n_{decay} = 400$, $A = 300\,V/m$.

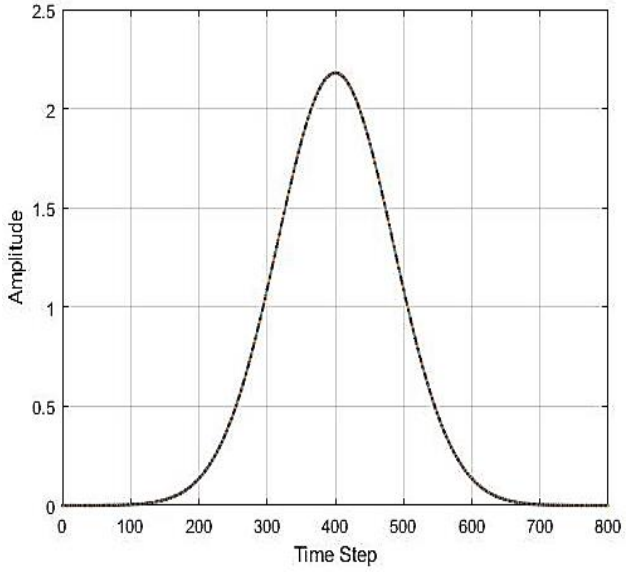

Figure 3.8 Time-domain Gaussian pulse at 2100MHz

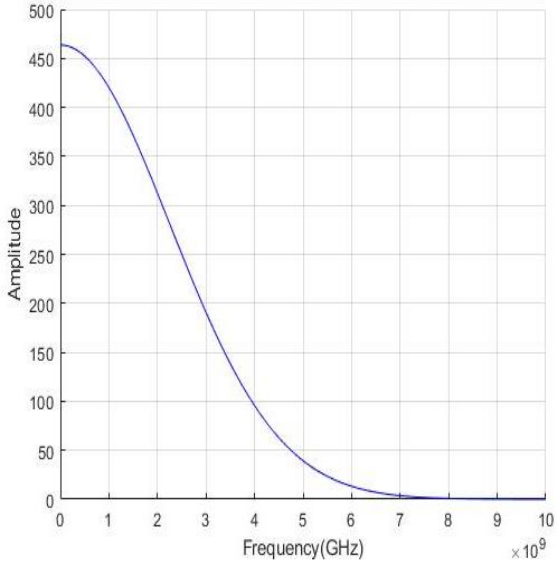

Figure 3.9 Fourier transform of 2100MHz Gaussian pulse

4. Frequency=2300MHz, E_0 =2.38, $n_0 = 120$,$n_{decay} = 400$, $A = 300\,V/m$.

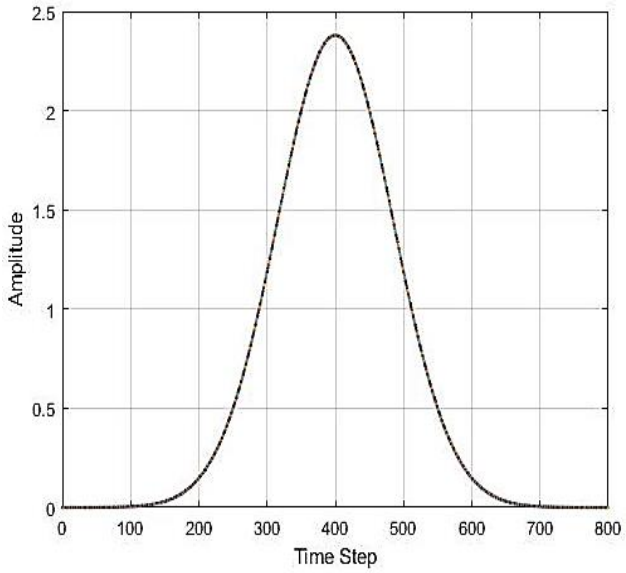

Figure 3.10 Time-domain Gaussian pulse at 2300MHz

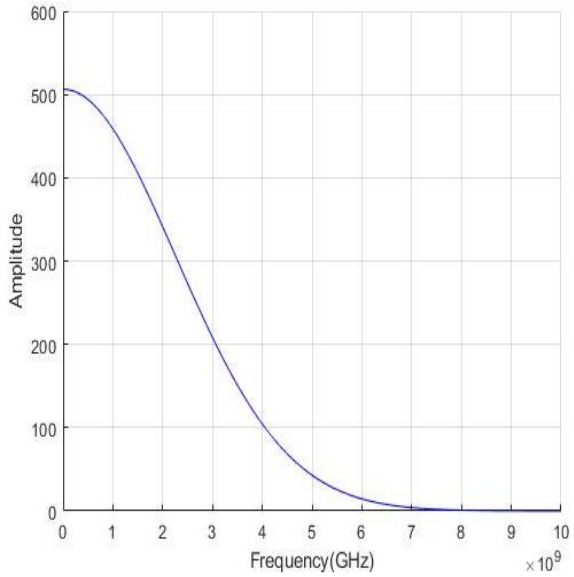

Figure 3.11 Fourier transform of 2300MHz Gaussian pulse

5. Frequency=2600MHz, $E_0 = 2.75$, $n_0 = 120$,$n_{decay} = 400$, $A = 300\,V/m$.

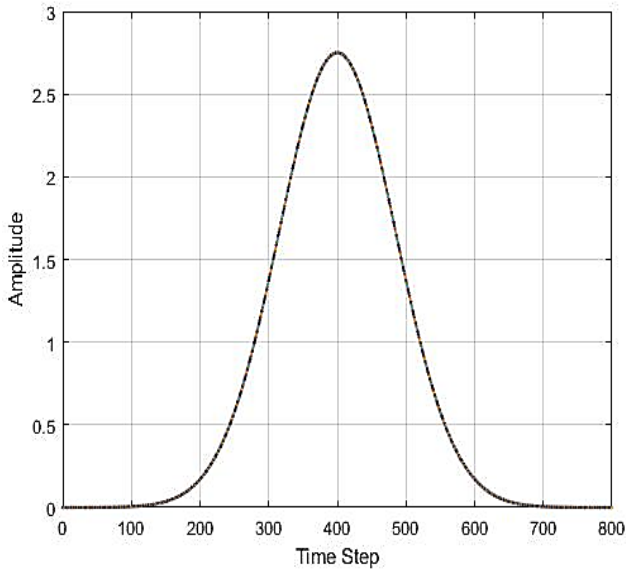

Figure 3.12 Time-domain Gaussian pulse at 2600MHz

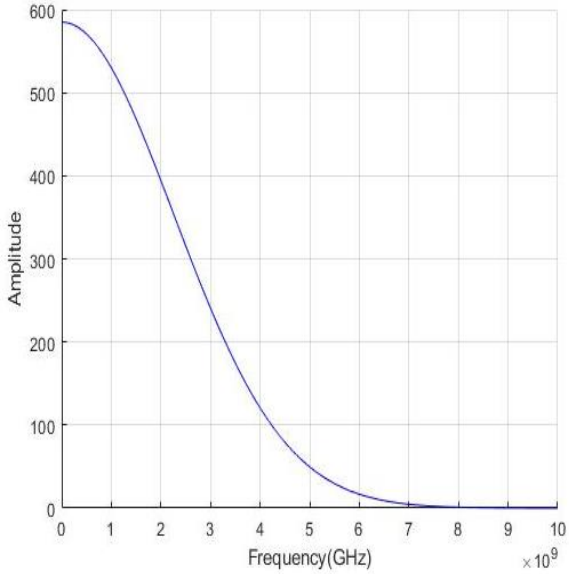

Figure 3.13 Fourier transform of 2600MHz Gaussian pulse

According to Figures 3.4-13, E_0 increases with the increase of frequency. Hence, it makes sense to compare the SAR level at different frequencies only when the input sources are the same. Different SAR levels are compared in this context considering the highest power that the mobile phone can generate to take into account worst-case scenarios. Only when such scenarios do not exceed the standard threshold, the exposure can be considered safe.

4. ADULT HEAD MODEL

4.1 SAR Results

With the use of the FDTD method, SAR distributions are found. Figures 4.1-4.6 show the results for nine frequencies: 0.7 GHz, 0.85 GHz, 0.9 GHz, 1.8 GHz, 2.1 GHz, 2.3 GHz, and 2.6 GHz.

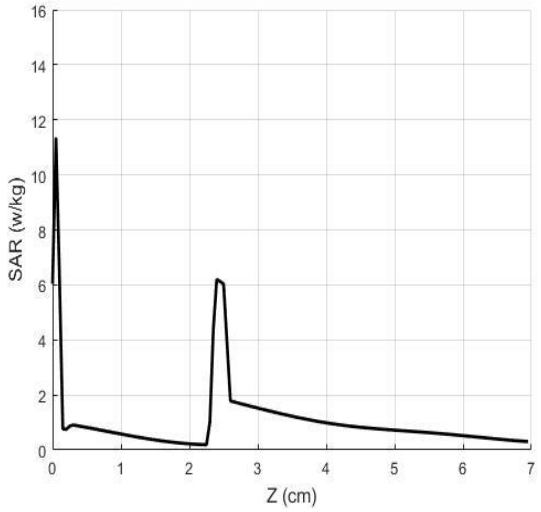

Figure 4.1 SAR of adult head model at 0.7 GHz

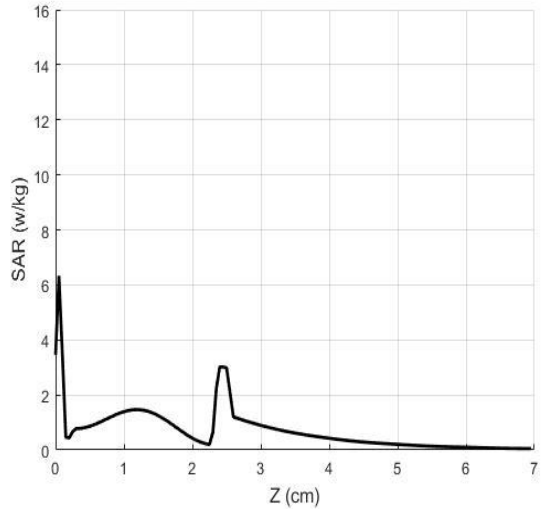

Figure 4.3 SAR of adult head model at 2.1 GHz

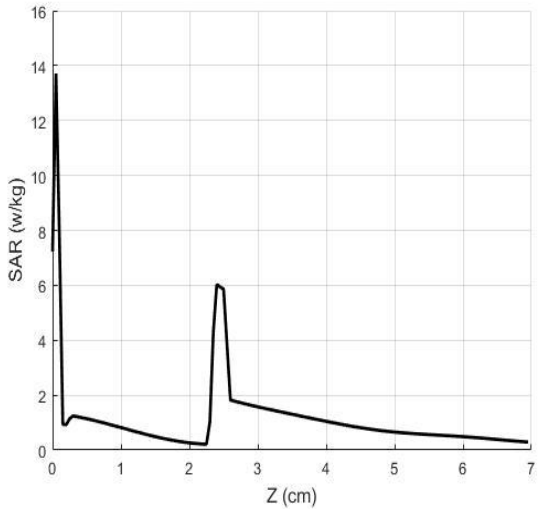

Figure 4.2 SAR of adult head model at 0.85 GHz

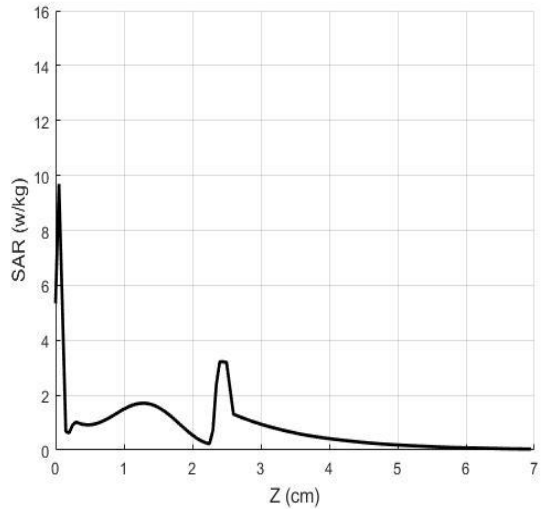

Figure 4.4 SAR of adult head model at 2.3 GHz

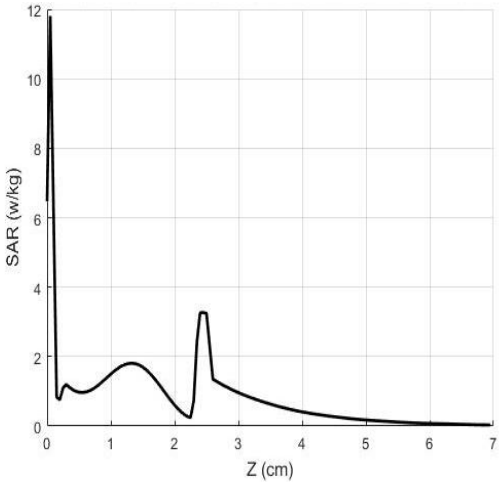

Figure 4.5 SAR of adult head model at 2.4 GHz

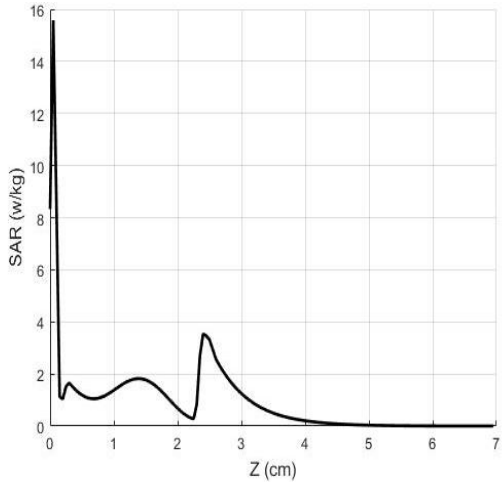

Figure 4.6 SAR of adult head model at 2.6 GHz

Since the skin and the CSF have a relatively high conductivity, and the skin also has such a thin layer (i.e., 0.07 cm), the skin and the CSF will have high SAR levels. Moreover, in the process of testing and simulating mobile phones, the first consideration should be the SAR of the skin layer, since it has the highest SAR. Keeping the SAR of the skin below the standard threshold will guaranteed the overall head to be safe.

As Figures 4.1-6 show, a higher frequency causes a higher conductivity, and the value of SAR increases with conductivity increases. Table 4.1 lists the peak values of SAR in adult human model in different layers.

It is noteworthy to point out that, SAR does not demonstrate the change in the head internal temperature caused by the duration of use. After using the phone for a long time, different thermal effects will change inside the head. This aspect is studied in this thesis with the use of the Pennes bioheat model.

Table 4.1 Peak SAR values of different layer

Freq (GHz) / **Tissue**	**Peak SAR Value** (W/Kg)							
	0.7	**0.85**	**0.9**	**1.8**	**2.1**	**2.3**	**2.4**	**2.6**
Skin	11.6	14.1	14.67	5.09	6.193	9.284	11.8	15.92
CSF	5.92	6.094	6.12	2.97	2.71	3.141	3.3	3.276
Brain	1.66	1.791	1.897	1.036	1.078	1.147	1.27	1.982

Table 4.2 The thermal parameters of the head tissues

Matter	Skin	Fat	Bone	Dura	CSF	Brain
$\boldsymbol{K}$ W/km	0.42	0.25	0.39	0.5	0.62	0.535
$\boldsymbol{C_p}$ $J/(K.kg)$	3600	3000	3100	3600	4000	3650
$\boldsymbol{B}$ W/km^3	9100	1700	1850	1125	0	40000

4.2 Short-term Peak Temperature

4.2.1 Pennes Model of the Bioheat Equation (BHE)

Describe the thermal interaction between tissue and perfused blood by using a quantitative basis is the concept published by Pennes [32] in 1948. The standard thermal diffusion equation given by Pennes shows as follows:

$$C_p(x)\rho(z)\frac{\partial T(x,t)}{\partial t} = K(x)\nabla^2 T(x,t) + \rho(x)SAR(x) - B(x)(T(x,t) - T_b) \quad (4.1)$$

where T is tissue temperature, K is thermal conductivity $(W/(K.m))$, ρ is tissue density (Kg/m^3), C_p is the specific heat capacity $(J/(K.Kg))$, x is the dimensional step, and T_b is the temperature of the blood. The values of K, C_p , and B list in Table 4.2[18].

The boundary conditions in the BHE as represented as follows:

$$K(x_{min})\frac{\partial T(x,t)}{\partial z} = -h(T(x,t) - T_a) + SW(x, T(x,t)) \quad (4.2)$$

where h is the coefficient of heat transfer, and T_a is the air temperature.

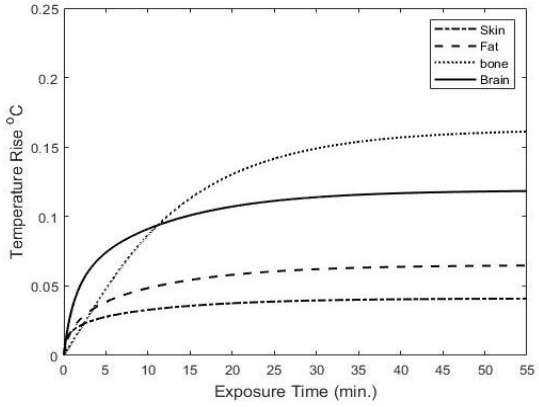

Figure 4.7 Temperature rise of different tissues at 700 MHz

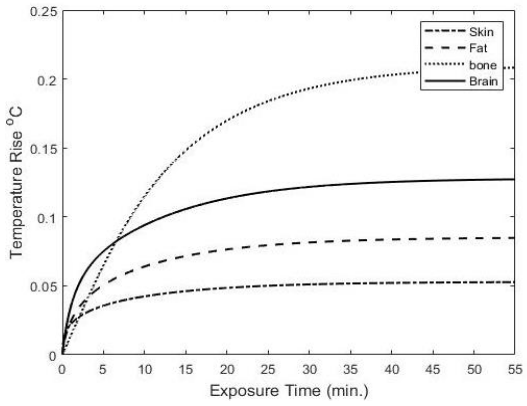

Figure 4.8 Temperature rise of different tissues at 850 MHz

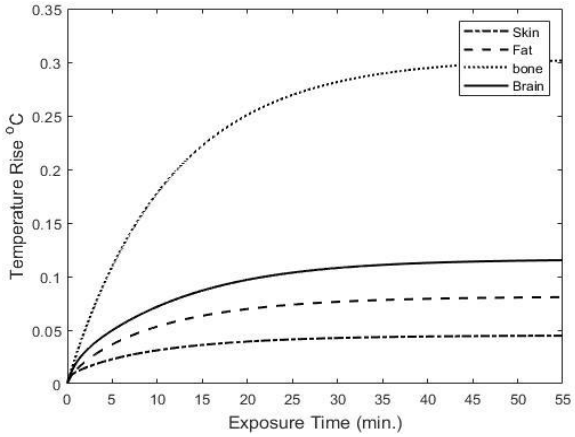

Figure 4.9 Temperature rise of different tissues at 2100 MHz

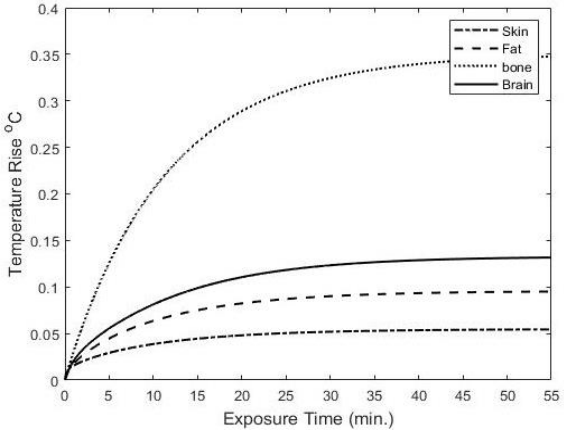

Figure 4.10 Temperature rise of different tissues at 2300 MHz

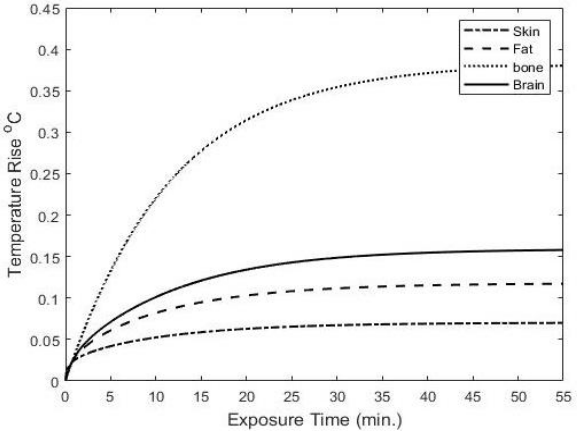

Figure 4.11 Temperature rise of different tissues at 2600 MHz

Figures 4.7 to 4.11 show the process of temperature rise in different layers at different frequencies. The results show that the temperature of the head material will increase exponentially when it is first exposed to radiation, and then the rate of temperature increase will slow down and slowly approach a stable value. At the same time, it is found that it requires more time to bring the brain temperature to a steady state as the frequency increases. Therefore, at high frequencies, the damage to the child's brain is reduced.

5. CHILD HEAD MODEL

According to the existing research, children and adolescents absorb EM radiation doses higher than adults. Radio frequency radiation has been classified as a category 2B carcinogen by the International Agency for Research on Cancer (IARC). It is thus important to accurately assess the dose of radiation absorbed by children and adolescents in their daily lives.

As the age increases, the water content of human tissues and organs decreases, and the coefficients of electrical conductivity and relative dielectric constant are also affected.

In 1980, Gabriel et al. [33] used experimental measurements to determine the electrical conductivity and relative permittivity of common tissues and organs in adults in the 10 Hz to 20 GHz band. These measurements are widely used to evaluate adults' radiation exposure.

In 1982, Dahdouh et al. [34] calculated the radiation doses absorbed by adult tissues/organs and children's tissues/organs and found that the parameters of the children's tissues/organs increase SAR levels of children's brains.

In 2009, Peyman et al. [35] considered that the media characteristics of sow tissues of specific age and weight age groups are similar (e.g., children of 1 to 4 years old, and children 11 to 13).

In 2012, Peyman et al. [36] measured the dielectric properties of rat embryo materials of different stages at 40MHz-20GHz. The results show that the fetal muscle and brain dielectric properties are generally higher than the adult group.

Therefore, these conductivity and relative permittivity can be used for SAR absorption rates in children of different grades.

5.1 Properties of different age head models

5.1.1 Conductivity and relative permittivity of each tissue under different ages

According to reference [33]-[44], the relative permittivity, ε_r is expressed in the following form:

$$\varepsilon_r = \varepsilon_r' - j\varepsilon_r'' = \varepsilon_r - j\frac{\sigma}{\omega\varepsilon_0} = \varepsilon_r(1 - j\frac{1}{\omega\tau}) \tag{5.1}$$

where ε_0 is vacuum permittivity (8.85×10^{-12} F/m), $\omega = 2\pi f$, and $\tau = \frac{\varepsilon_0\varepsilon_r}{\sigma}$.

Since dielectric properties are changed based on age, the formula can be represented as follows:

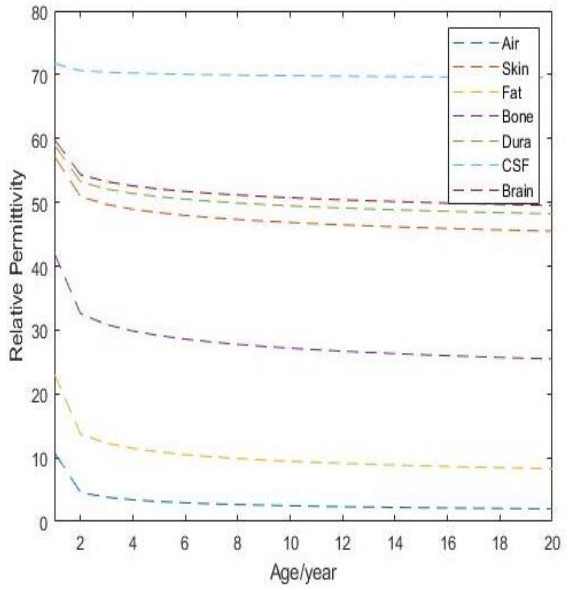

Figure 5.1 The relative permittivity of 7 tissues of various ages at 900 MHz

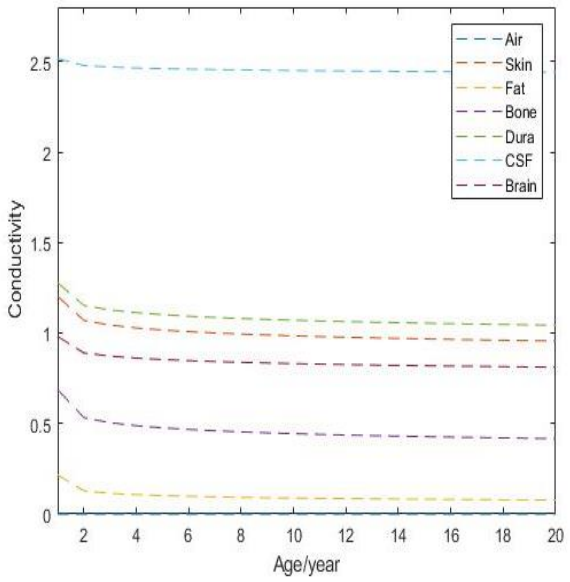

Figure 5.2 The conductivity of 7 tissues of various ages at 900 MHz

$$\varepsilon_r = \varepsilon_{rw}^{\frac{\alpha-\alpha_A}{1-\alpha_A}} \cdot \varepsilon_{rA}^{\frac{1-\alpha}{1-\alpha_A}}(1 - j\frac{1}{\omega\tau}) \tag{5.2}$$

where ε_{rw} is the property of water, $\varepsilon_{rw} = 74.3$ (37℃), ε_{rA} is the relative permittivity of adult, α is the hydrated rate, shows as follows:

$$\alpha = \rho \cdot TBW \tag{5.3}$$

$$TBW = 784 - 241e^{-(\frac{In(age/55)}{6.9589})^2} \tag{5.4}$$

In addition, ρ is tissue density, which is the adult tissue density. α_A is the hydrated rate of an adult, TBW is total body water, and the unit of age is year.

The Figure 5.1-5.2 shows both the ε_r and σ are decreased with the increasing age. The significant change range is from new-born to 2-years-old. They are gradually tending to a fixed value with age, which is the value of adults.

Table 5.1- 5.15 list the conductivity and relative permittivity values of 1-day-old, 6-months-old, 1-year-old, 3-years-old, 7-years-old, 10-years-old and adult at different frequencies.

Table 5.1 The conductivity of different ages at 700MHz

Tissue / Age	Conductivity					
	Skin	**Fat**	**Bone**	**Dura**	**CSF**	**Brain**
1 day	1.044	0.164	0.538	1.147	2.422	0.868
6 months	0.895	0.080	0.380	0.998	2.374	0.763
1 year old	0.872	0.071	0.359	0.975	2.366	0.747
3 years old	0.840	0.059	0.330	0.943	2.355	0.724
7 years old	0.821	0.053	0.313	0.923	2.348	0.710
10 years old	0.814	0.051	0.307	0.917	2.345	0.705
Adult	0.800	0.047	0.295	0.902	2.340	0.695

Table 5.2 The relative permittivity of different ages at 700MHz

Tissue / Age	Relative Permittivity					
	Skin	**Fat**	**Bone**	**Dura**	**CSF**	**Brain**
1 day	55.70	19.17	38.76	57.24	71.58	58.42
6 months	47.77	9.31	27.40	49.80	70.17	51.39
1 year old	46.55	8.25	25.85	48.66	69.94	50.30
3 years old	44.85	6.92	23.76	47.04	69.60	48.75
7 years old	43.81	6.20	22.54	46.06	69.39	47.81
10 years old	43.47	5.98	22.15	45.73	69.32	47.50
Adult	42.70	5.50	21.27	45.00	69.16	46.80

Table 5.3 The conductivity of different ages at 850MHz

Tissue / Age	Conductivity					
	Skin	**Fat**	**Bone**	**Dura**	**CSF**	**Brain**
1 day	1.122	0.175	0.329	1.214	2.481	0.944
6 months	1.023	0.115	0.248	1.119	2.450	0.874
1 year old	0.930	0.075	0.185	1.029	2.419	0.808
3 years old	0.895	0.063	0.164	0.994	2.406	0.783
7 years old	0.873	0.056	0.152	0.973	2.399	0.767
10 years old	0.866	0.054	0.148	0.966	2.396	0.762
Adult	0.851	0.050	0.140	0.951	2.390	0.751

Table 5.4 The relative permittivity of different ages at 850MHz

Tissue / Age	Relative Permittivity					
	Skin	**Fat**	**Bone**	**Dura**	**CSF**	**Brain**
1 day	55.00	19.13	29.40	56.94	71.36	57.91
6 months	50.15	12.61	22.11	52.47	70.48	53.64
1 year old	45.61	8.22	16.51	48.25	69.59	49.59
3 years old	43.87	6.89	14.64	46.62	69.22	48.01
7 years old	42.81	6.17	13.58	45.62	69.00	47.05
10 years old	42.46	5.95	13.24	45.29	68.92	46.74
Adult	41.72	5.49	12.54	44.59	68.76	46.06

Table 5.5 The conductivity of different ages at 900MHz

Tissue / Age	Conductivity					
	Skin	**Fat**	**Bone**	**Dura**	**CSF**	**Brain**
1 day	1.152	0.178	0.330	1.229	2.502	0.946
6 months	1.049	0.118	0.248	1.132	2.471	0.876
1 year old	0.953	0.077	0.185	1.040	2.440	0.809
3 years old	0.916	0.064	0.164	1.005	2.427	0.783
7 years old	0.894	0.058	0.152	0.983	2.419	0.767
10 years old	0.887	0.055	0.148	0.976	2.416	0.762
Adult	0.871	0.051	0.140	0.961	2.410	0.751

Table 5.6 The relative permittivity of different ages at 900MHz

Tissue / Age	Relative Permittivity					
	Skin	**Fat**	**Bone**	**Dura**	**CSF**	**Brain**
1 day	54.82	19.11	29.34	56.84	71.33	57.77
6 months	49.93	12.59	22.05	52.35	70.44	53.47
1 year old	45.36	8.20	16.45	48.11	69.54	49.39
3 years old	43.61	6.88	14.58	46.47	69.18	47.81
7 years old	42.55	6.16	13.53	45.47	68.95	46.84
10 years old	42.20	5.94	13.19	45.14	68.87	46.52
Adult	41.45	5.48	12.49	44.44	68.71	45.84

Table 5.7 The conductivity of different ages at 1800MHz

Tissue / Age	Conductivity					
	Skin	**Fat**	**Bone**	**Dura**	**CSF**	**Brain**
1 day	1.610	0.276	0.677	1.718	3.064	1.487
6 months	1.451	0.181	0.505	1.574	3.015	1.365
1 year old	1.305	0.118	0.373	1.438	2.966	1.250
3 years old	1.250	0.098	0.330	1.386	2.946	1.206
7 years old	1.216	0.088	0.305	1.354	2.934	1.179
10 years old	1.205	0.085	0.297	1.344	2.929	1.170
Adult	1.181	0.078	0.281	1.321	2.920	1.151

Table 5.8 The relative permittivity of different ages at 1800MHz

Tissue / Age	Relative Permittivity					
	Skin	**Fat**	**Bone**	**Dura**	**CSF**	**Brain**
1 day	53.06	18.89	28.53	55.83	70.52	56.24
6 months	47.85	12.40	21.26	51.14	69.39	51.63
1 year old	43.03	8.05	15.72	46.74	68.26	47.29
3 years old	41.20	6.74	13.89	45.04	67.80	45.61
7 years old	40.09	6.03	12.85	44.01	67.51	44.59
10 years old	39.72	5.81	12.52	43.67	67.42	44.26
Adult	38.94	5.36	11.83	42.94	67.21	43.54

Table 5.9 The conductivity of different ages at 2100MHz

Tissue / Age	Conductivity					
	Skin	**Fat**	**Bone**	**Dura**	**CSF**	**Brain**
1 day	1.797	0.319	0.805	1.922	3.316	1.702
6 months	1.618	0.209	0.598	1.758	3.260	1.560
1 year old	1.452	0.136	0.441	1.604	3.203	1.426
3 years old	1.389	0.114	0.389	1.545	3.180	1.375
7 years old	1.351	0.102	0.360	1.509	3.166	1.344
10 years old	1.338	0.098	0.350	1.497	3.161	1.333
Adult	1.311	0.090	0.331	1.471	3.151	1.311

Table 5.10 The relative permittivity of different ages at 2100MHz

Tissue / Age	Relative Permittivity					
	Skin	**Fat**	**Bone**	**Dura**	**CSF**	**Brain**
1 day	52.73	18.85	28.26	55.56	70.28	55.94
6 months	47.46	12.37	21.00	50.81	69.09	51.27
1 year old	42.59	8.03	15.49	46.36	67.88	46.88
3 years old	40.74	6.72	13.66	44.65	67.40	45.19
7 years old	39.62	6.01	12.63	43.61	67.09	44.16
10 years old	39.25	5.79	12.30	43.26	66.99	43.82
Adult	38.47	5.34	11.62	42.53	66.77	43.10

Table 5.11 The conductivity of different ages at 2300MHz

Tissue / Age	Conductivity					
	Skin	**Fat**	**Bone**	**Dura**	**CSF**	**Brain**
1 day	1.920	0.348	0.907	2.072	3.502	1.851
6 months	1.726	0.228	0.673	1.893	3.440	1.695
1 year old	1.548	0.148	0.495	1.726	3.378	1.548
3 years old	1.480	0.124	0.437	1.661	3.353	1.491
7 years old	1.439	0.111	0.404	1.622	3.337	1.457
10 years old	1.425	0.107	0.393	1.609	3.332	1.445
Adult	1.396	0.098	0.371	1.581	3.321	1.421

Table 5.12 The relative permittivity of different ages at 2300MHz

Tissue / Age	Relative Permittivity					
	Skin	**Fat**	**Bone**	**Dura**	**CSF**	**Brain**
1 day	52.55	18.81	28.11	55.38	70.12	55.73
6 months	47.25	12.34	20.86	50.60	68.88	51.02
1 year old	42.36	8.00	15.35	46.12	67.63	46.60
3 years old	40.50	6.70	13.53	44.40	67.13	44.90
7 years old	39.38	5.99	12.51	43.35	66.81	43.86
10 years old	39.01	5.77	12.18	43.00	66.71	43.52
Adult	38.22	5.32	11.50	42.27	66.48	42.79

Table 5.13 The conductivity of different ages at 2400MHz

Tissue / Age	Conductivity					
	Skin	**Fat**	**Bone**	**Dura**	**CSF**	**Brain**
1 day	1.985	0.362	0.946	2.153	3.601	1.933
6 months	1.784	0.238	0.701	1.966	3.536	1.768
1 year old	1.598	0.154	0.516	1.791	3.471	1.614
3 years old	1.528	0.129	0.455	1.724	3.444	1.555
7 years old	1.485	0.115	0.420	1.683	3.428	1.519
10 years old	1.471	0.111	0.409	1.669	3.422	1.507
Adult	1.442	0.102	0.386	1.640	3.411	1.481

Table 5.14 The relative permittivity of different ages at 2400MHz

Tissue / Age	Relative Permittivity					
	Skin	**Fat**	**Bone**	**Dura**	**CSF**	**Brain**
1 day	52.46	18.80	28.04	55.29	70.04	55.64
6 months	47.14	12.32	20.78	50.49	68.78	50.91
1 year old	42.25	7.99	15.28	46.00	67.51	46.47
3 years old	40.38	6.69	13.47	44.27	66.99	44.76
7 years old	39.26	5.98	12.45	43.23	66.67	43.72
10 years old	38.89	5.76	12.12	42.88	66.56	43.38
Adult	38.10	5.31	11.44	42.14	66.33	42.65

Table 5.15 The conductivity of different ages at 2600MHz

Tissue / Age	Conductivity					
	Skin	**Fat**	**Bone**	**Dura**	**CSF**	**Brain**
1 day	2.128	0.392	1.037	2.318	3.810	4.192
6 months	1.911	0.257	0.768	2.115	3.739	3.831
1 year old	1.711	0.166	0.563	1.925	3.667	3.493
3 years old	1.635	0.139	0.496	1.852	3.638	3.364
7 years old	1.589	0.124	0.458	1.808	3.620	3.285
10 years old	1.574	0.120	0.446	1.793	3.614	3.258
Adult	1.542	0.110	0.421	1.762	3.601	3.203

Table 5.16 The relative permittivity of different ages at 2600MHz

Tissue / Age	Relative Permittivity					
	Skin	**Fat**	**Bone**	**Dura**	**CSF**	**Brain**
1 day	52.31	18.74	27.88	55.11	69.87	55.45
6 months	46.97	12.27	20.63	50.28	68.56	50.68
1 year old	42.05	7.95	15.15	45.76	67.25	46.21
3 years old	40.18	6.65	13.34	44.02	66.71	44.49
7 years old	39.05	5.95	12.32	42.97	66.38	43.45
10 years old	38.68	5.73	12.00	42.62	66.27	43.10
Adult	37.89	5.28	11.32	41.88	66.03	42.37

5.1.2 Child head model based on various ages [45-49]

According to reference [45-49], a child head model is generated based on age. There are six layers in the adult model. In order to make the result more accurate and to make the head model much closer to the actual one, the scaling factor of each layer is calculated separately.

For fat layer, since the bone of the child's head is not strong enough in the neonatal period, the proportion of head fat in infants and young kids are even higher than adults to protect the child 's head and protect future development. The thickness of fat layer in adult head model is 0.07 cm. For a 6-month-old infant, the scaling of fat layer is 2.28, so the thickness is equal to 0.16 cm; for an 1-year-old child, the scaling of fat layer is 1.85, and fat layer is 0.13cm; for a 3-years-old child, the scaling of fat layer, the thickness of fat layer is such close to adult model. Therefore, the difference between them are negligible.

For skin, bone, and Dura layer, a general scaling is applied. The scaling factors of 6-months-old, 1-year-old, 3-years-old, and 7-years old are 0.465, 0.536, 0.618, and 0.706.

For grey matter, the relationship between the age factor, *AF*, and the volume of grey matter shows as follows:

$$Grey\ Matter = 653 - 33.54 \times AF \tag{5.5}$$

$$AF = \frac{1}{\sqrt{a/100}} - 1.462 \tag{5.6}$$

where a is age, unit by month.

For white matter based on a new *AF* (separate in each material), the volume of white matter shows as follows:

$$White\ Matter = 298 + 72.74 \times AF \tag{5.7}$$

Table 5.17 Age-based white-matter, CSF, and grey-matter scaling

Age/Tissue	White-matter		Grey-matter		CSF	
	Volume	**Scaling**	**Volume**	**Scaling**	**Volume**	**Scaling**
6-month-old	148.89	0.37	366.53	0.56	121.33	0.705
1-year-old	199.3	0.498	605.21	0.923	130.97	0.76
3-years-old	279.22	0.698	646.13	0.989	146.27	0.85
7-years-old	340.85	0.852	650.44	0.996	156.52	0.91
Adult	400	1	653	1	172	1

$$AF = \ln\left(\frac{a}{100}\right) + 0.7596 \tag{5.8}$$

For CSF, the relationship between a and the volume of CSF shows as follows:

$$CSF = 149.88 + 13.90 \times AF \tag{5.7}$$

$$AF = \ln\left(\frac{a}{100}\right) + 0.7596 \tag{5.8}$$

Table 5.17 represents the actual value of each tissue; the scaling of each tissue is applied to the child head model. There is one thing to note that in the six-layered model, white matter layer and grey matter layer are combined to a whole brain layer. Therefore, the average of white matter and grey matter are applied to brain value (i.e., conductivity, relative permittivity, scaling, tissue density).

Figure 5.3 shows the trend of tissues with age, which shows a rapid growth in the interval from zero to two years old, and it tends to a fixed value with increasing age. In addition, the fixed value here is the representative of the adult value.

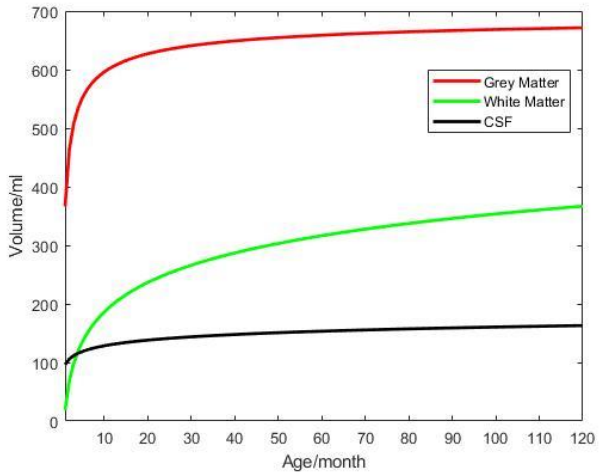

Figure 5.3 Volume of tissues (i.e., grey matter, white matter, and CSF) based on age

5.2 Comparison of human and child head model result

5.2.1 SAR Results

In order to maintain a fair comparison, all input sources are set such that the SAR of the adult at the skin layer is 2 W/kg. Then, such sources are applied to all age groups and frequencies.

According to Figure 5.4, the results show that the SAR level at the skin in the children's head at all ages exceeds the standard threshold (2 W/Kg). Furthermore, at the same frequency, the younger the age, the larger the SAR value. In addition, for a given age, it is found that when the frequency increases, the SAR value also increases.

Table 5.18 show the exact value of SAR value in skin, CSF, and brain. It compares the SAR values of different ages in various frequencies.

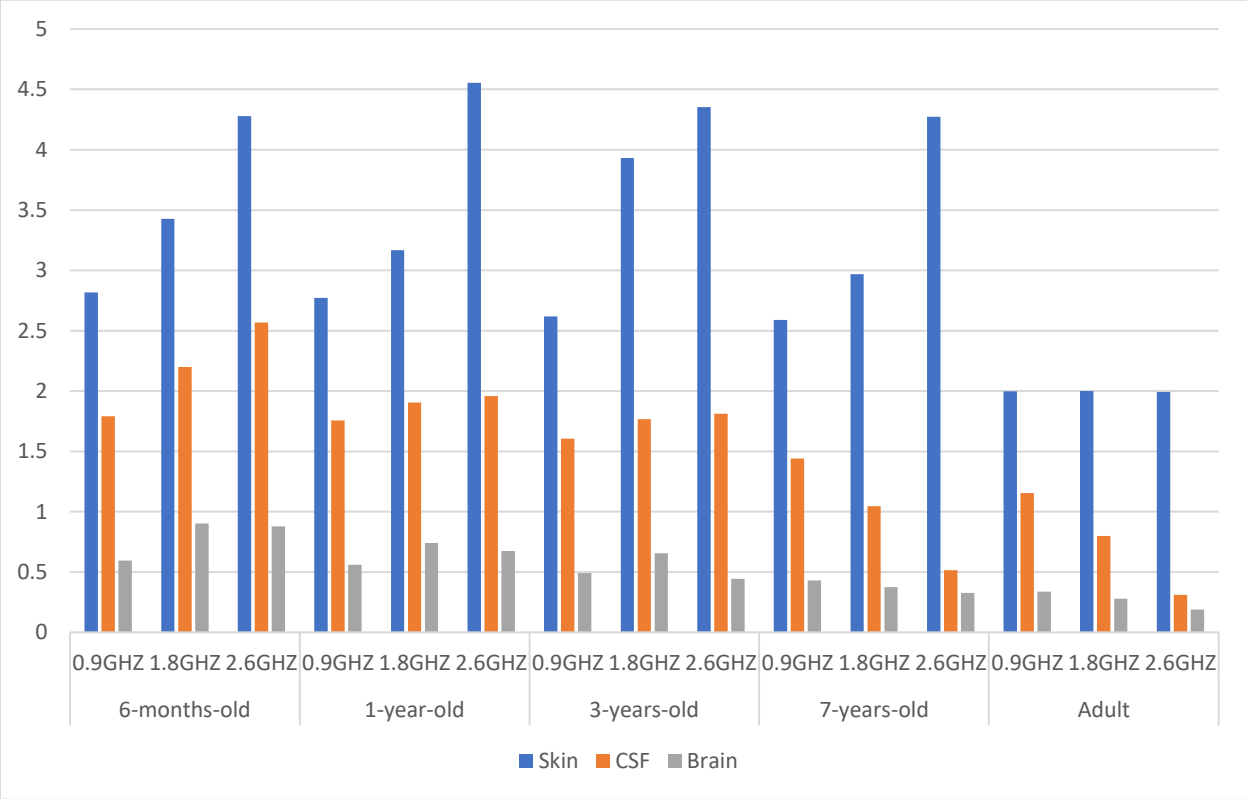

Figure 5.4 Comparison of SAR values for different age considering 900MHz,1800MHz, and 2600MHz

Table 5.18 The SAR value of different age in 0.9GHz,1.8GHz, 2.6GHz

Age/Tissue		Skin	CSF	Brain
6 months	0.9GHZ	2.817	1.792	0.5946
	1.8GHZ	3.426189	2.199646	0.902848
	2.6GHZ	4.279138	2.56884	0.879598
1 year	0.9GHZ	2.772	1.756	0.5595
	1.8GHZ	3.167913	1.905777	0.741424
	2.6GHZ	4.554462	1.9566	0.675208
3 year	0.9GHZ	2.618	1.605	0.4919
	1.8GHZ	3.930754	1.766538	0.655582
	2.6GHZ	4.352077	1.8116	0.442252
7 year	0.9GHZ	2.589	1.440	0.430
	1.8GHZ	2.968	1.045	0.376
	2.6GHZ	4.273	0.515	0.327
Adult	0.9GHZ	1.997	1.155	0.337
	1.8GHZ	2.000	0.800	0.279
	2.6GHZ	1.992	0.310	0.188

From Figure 5.5, The trend of SAR change can be seen intuitively. The adult SAR is recalled for comparison purposes. Due to the use of head models for different ages, each layer thickness in each age is reduced (i.e., scaled) by a specific proportion.

In conclusion, children exposed to EM radiation develop higher SAR averages in comparison to adult.

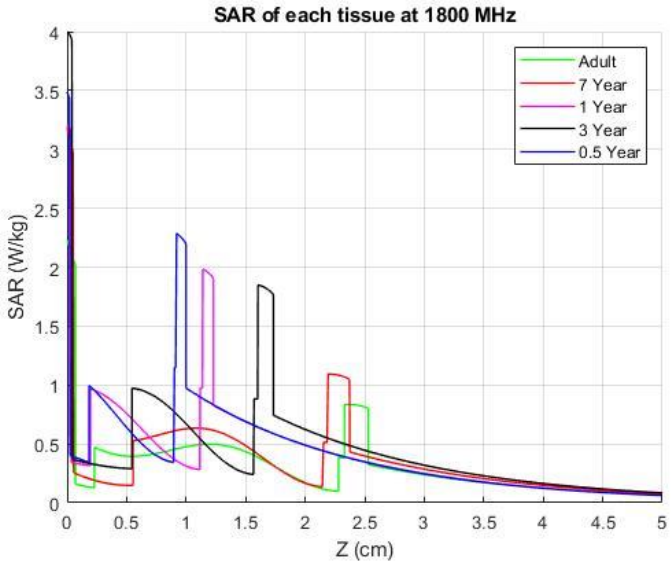

Figure 5.5 Distribution of SAR in the brain at different ages at 1800MHz

5.2.2 **Short-term peak temperature rise**

Figure 5.6-5.9 show how the thermal effects of different materials on the time axis for different tissues of 6 months, 1 year, 3 years, and adult in 900MHz. The same as expected, the younger the child is, the stronger the thermal effect shows in the head. Additionally, the excitation source used in the following result is also adjusted to reach 2W/kg at skin layer.

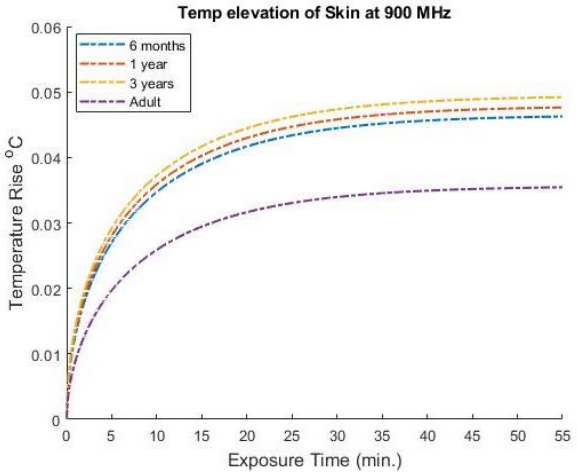

Figure 5.6 Temp rise in Skin at 900MHz

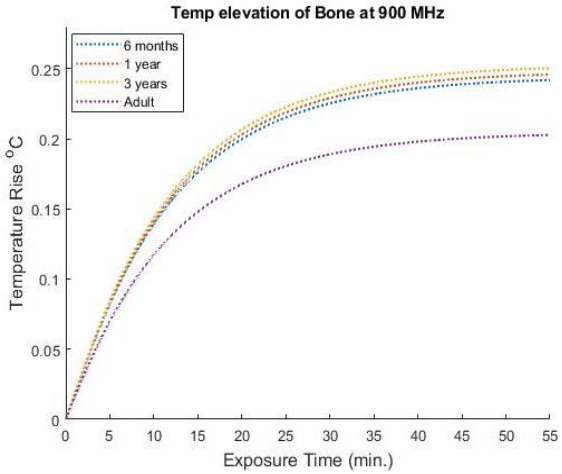

Figure 5.8 Temp rise in bone at 900MHz

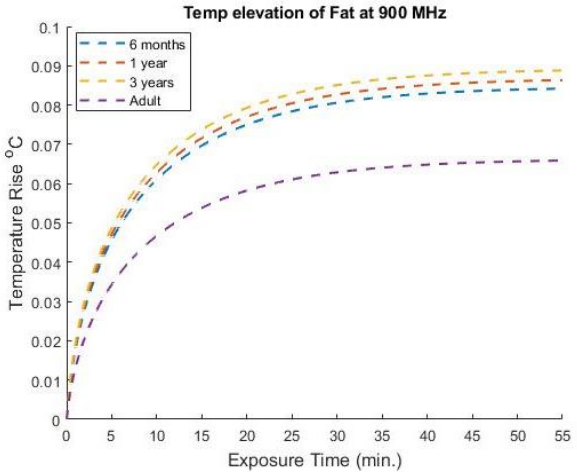

Figure 5.7 Temp rise in fat at 900MHz

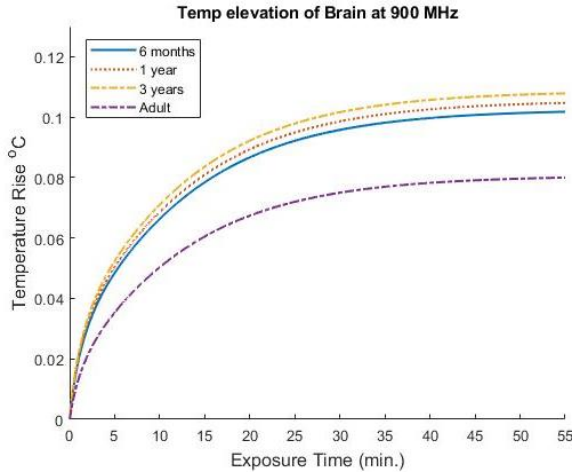

Figure 5.9 Temp rise in brain at 900MHz

6. CONCLUSION AND FUTURE WORK

In general, this thesis has demonstrated the specific absorption rate distribution of the adult head at different frequencies on the two-dimensional plane and the distribution map of the thermal effect in the head caused by the absorption of radiation by different tissues. At the same time, we also studied the different results of adults and children due to different ages and compared them. The results show that under the same age, the specific absorption rate of the head will continue to increase with the increase of frequency, and the increase rate of the skin surface layer is the largest. And when we control the input source to be consistent and satisfy the adult skin (the highest specific absorption rate of each material in the head), the effective absorption rate reaches the threshold, which is 2W/kg, we find that as the age continues to decrease, the effective absorption The rate increases continuously as a whole, and also increases as the frequency increases. This shows that child is more sensitive to EM radiation and more vulnerable to injury, and they should be kept away from the use of electronic equipment.

In addition, the current limit value based on the SAR of adults used in various countries is not perfect. The head of an adult is essentially different from that of a child. Therefore, when formulating rules, consideration should be given to different factors Different specific absorption rates due to age. Especially, some electronic equipment produced for infants and children should have a set of targeted standards. From another point of view, at the parent level, the frequency and time of children's use of electronic products should be controlled, especially during the infant period.

In the future research, the MRI-3D head model obtained from the actual experiment will be used relative to the theoretically two-dimensional plane, so that the experiment can be judged according to the thermal imaging changes actually occurred when the simulated head uses the mobile phone. Moreover, as the number of head model samples increases, the experimental results will be more accurate. Furthermore, this research is aimed at mobile phones. If we change the signal source, we can study the impact of different electronic products on the human body.

If we use the actual 3D model, then we will no longer be limited to the head model. In the future, wearable full-body electronic module devices have become a trend. If we can get the specific data of the entire human body through 3D modeling, the real specific absorption rate will be visualized.

With the continuous development of communication technology, future research will also involve high frequency bands, which will have a big gap between each generation of communication technology. At that point, how to achieve the same standards as low frequency bands in high frequency bands will be studied.

APPENDIX

Acronyms

FDTD	Finite Difference Time Domain
ANSI	American National Standard Institution
EM	Electromagnetic
RF	Radio Frequency
IEEE	Institution of Electrical and Electronic Engineering
WHO	World Health Organization
ITU	International Telecommunication Union
GTD	Geometric Theory of Diffraction
BHE	Bioheat Equation
SAR	Specific Absorption Rate
ICNIRP	International Commission on Non-Ionizing Radiation Protection

REFERENCES

[1] Beir. V," Health Effects of Exposure to Low Levels of Ionizing Radiation", Washington (DC): National Academies Press (US); 1990., ISBN-10: 0-309-03995-9

[2] Kenneth R. Foster & Joseph J. Morrissey (2011) Thermal aspects of exposure to radiofrequency energy: Report of a workshop, International Journal of Hyperthermia, 27:4, 307-319, DOI:10.3109/02656736.2010.545965

[3] Moneda, A.P., Ioannidou, M.P., Chrissoulidis, D.P., "Radio-wave exposure of the human head: analytical study based on a versatile eccentric spheres model including a brain core and pair of eyeballs", IEEE Trans. Biomed. Eng., 2003, 50, (6), pp. 667–676.

[4] W. Zhi, L Wang "Recent advances in the effects of microwave radiation on brains", Beijing Institute of Radiation Medicine, Beijing, 2017

[5] P. French, R. Penny, "Mobile phones, heat shock proteins and cancer", Differentiation 67(4-5):93-7., DOI: 10.1046/j.1432-0436.2001.670401. x., June 2001

[6] "IEC/IEEE International Standard -- Determining the peak spatial-average specific absorption rate (SAR) in the human body from wireless communications devices, 30 MHz to 6 GHz - Part 1: General requirements for using the finite-difference time-domain (FDTD) method for SAR calculations," in IEC/IEEE 62704-1:2017 , vol., no., pp.1-86, 27 Oct. 2017.

[7] "IEEE/IEC International Standard -- Determining the peak spatial-average specific absorption rate (SAR) in the human body from wireless communications devices, 30 MHz to 6 GHz -- Part 2: Specific requirements for finite difference time domain (FDTD) modelling of exposure from vehicle mounted antennas," in *IEC/IEEE 62704-2:2017* , vol., no., pp.1-112, 30 June 2017.

[8] Kuster, N., Schönborn, F., "Recommended minimal requirements and development guidelines for exposure setups of bio-experiments addressing the health risk concern of wireless communications", Bio electromagnetics, October 2000, Vol.21(7), pp.508-514

[9] G. Neubauer, G. Schmid, "SAR Evaluation in Human Heads", Austrian Research Center Seibersdorf.

[10] Tian Fang, Li Dongfeng FDTD method analysis of a new dual-frequency planar inverted-F mobile phone antenna, Journal of Communications, Volume 2, Issue 8.

[11] Zhou Xiaoming, Research on Modeling and Numerical Simulation of Mobile Phone and Human Body System, Ph.D. Thesis of South China University of Technology

[12] D. G. Choi, C. S. Shin, N. Kim, and H. S. Shin, "Design and SAR Analysis of Broadband PIFA with Triple Band", August 2005

[13] Oskooi A F, Roundy D, Ibanescu M, et al. "A flexible free-software package for electromagnetic simulations by the FDTD method. Computer Physics Communications", 2010, 181(3): 687-702.

[14] A.I. Sabbah, N.I. Dib, M.A. Al-Nimr, "Evaluation of specific absorption rate and temperature elevation in a multi-layered human head model exposed to radio frequency radiation using the finite-difference time domain method", IET Microwaves, Antennas & Propagation, April 2010

[15] Çapoğlu I R, Taflove A, Backman V. "A Free Software Package for Finite-Difference Time-Domain Electromagnetic Simulation." IEEE Antennas and Propagation Magazine, 2013, 55(4): 80-93.

[16] B. Mohammed, J. Jin, A. M. Abbosh, K. S. Bialkowski, M. Manoufali and S. Crozier, "Evaluation of Children's Exposure to Electromagnetic Fields of Mobile Phones Using Age-Specific Head Models with Age-Dependent Dielectric Properties," in IEEE Access, vol. 5, pp. 27345-27353, 2017.

[17] Abdalla A. and Teoh A., "A Multi Layered Model of Human Head Irradiated by Electromagnetic Plane Wave of 100MHz-300GHz," Int. J. Sci. Res., 15: 1-7, 2005.

[18] Moneda, A.P., Ioannidou, M.P., Chrissoulidis, D.P., "Radio-wave exposure of the human head: analytical study based on a versatile eccentric spheres model including a brain core and pair of eyeballs", IEEE Trans. Biomed. Eng., 2003, 50, (6), pp. 667–676.

[19] Dielectric properties of the body tissues: http://niremf.ifac.cnr.it/tissprop/htmlclie/htmlclie.php accessed April 2020.

[20] K. H. Joyner V. Anderson. Specific absorption rate levels measured in a phantom head exposed

to radio frequency transmissions from analog hand-held mobile phones. Bioelectromagnetic., V 16, pp. 60-69, 1995.

[21] Sullivan D., "Electromagnetic Simulation Using the FDTD Method", New York: IEEE Press, 2000.

[22] Taflove A., and Hagness S.,” Computational Electrodynamics: The Finite- Difference Time-Domain Method”, 2nd edition, Boston: Artech House, 2000.

[23] Kunz K. S., and Luebbers, R. J., “The Finite-Difference Time-Domain Method for Electromagnetics”, CRC, Boca Raton, FL, 1993.

[24] Elsherbeni A., and Demir V., “The Finite-Difference Time-Domain Method for Electromagnetics with MATLAB Simulations”, SciTech Inc., Raleigh, NC, 2009.

[25] Yang L., Bin L., Hiroyasu S., Qiang C., “Application of Electromagnetic Simulation Techniques based on FDTD Method in Human Body Healthcare”, 2018 International ACES, August 2018.

[26] Yanjun G., Jinxue H., “The FDTD modeling of body of revolution”, IEEE, July 2010.

[27] Valerio D.S., Mauro F., Francescaromana M., “Safety Assessment of UWB Radio Systems for Body Area Network by the FDTD Method”, Magnetics, IEEE Transactions, August 2010.

[28] A. Shafi, A. Hussain and J. Raza, "A parallel implementation of the Finite-Domain Time-Difference algorithm using MPJ express," 2008 IEEE International Symposium on Parallel and Distributed Processing, Miami, FL, 2008, pp. 1-6.

[29] A.D. Usman, W.F. Wan Ahmad., “Wireless Phones Electromagnetic Field Radiation Exposure Assessment”, American J. of Engineering and Applied Sciences 2 (4): 771-774, 2009

[30] R. Páez-Hernández., M. Zamora-Gómez., A. Ramírez-Rojas., J.M Velázquez-Arcos, “Electromagnetic field produced by a cell phone”, Oct.2015.

[31] Stephen W., ZhongMin W., Thomas K., Dina D., Michael L., “Real-world cell phone radiofrequency electromagnetic field exposures”, Environmental Research, Oct.2018.

[32] Pennes H. H., “Analysis of Tissue and Arterial Blood Temperatures in Resting Forearm,” Journal of Applied Physiology 1(2): 93–122, August 1948.

[33] Gabriel S, Lau R W, Gabriel C. “The dielectric properties of biological tissues: II. Measurements in the frequency range 10 Hz to 20 GHz.” Physics in Medicine &Biology, 1996.

[34] Dahdouh S, Varsier N, Ochoa M A N, “Infants and young children modeling method for numerical dosimetry studies: application to plane wave exposure”, Physics in Medicine & Biology, 2016.

[35] Peyman A, Gabriel C, Grant E H, “Variation of the dielectric properties of tissues with age: the effect on the values of SAR in children when exposed to walkie–talkie devices.”, Physics in Medicine & Biology, 2009, 54(2): 227.

[36] A. Peyman, C. Gabriel, “Cole–Cole parameters for the dielectric properties of porcine tissues as a function of age at microwave frequencies”, 2010 Institute of Physics and Engineering in Medicine, Jul.20.2010.

[37] A. Stogryn, "Equations for Calculating the Dielectric Constant of Saline Water (Correspondence)," IEEE Transactions on Microwave Theory and Techniques, vol. 19, no. 8, pp. 733-736, Aug.1971.

[38] Hirata A., Shirai K., and Fujiwara O., “On Averaging Mass of SAR Correlating with Temperature Elevation Due to Dipole Antenna,” Progress in Electromagnetics Research, PIER 84: 221–237, 2008.

[39] William. C. C, Shumei. S. G, Christine. M. Z, Nicholas. V. R, “Total body water reference values and prediction equations for adults”, Kidney International, Vol. 59 (2001), pp. 2250–2258

[40] Jianqing. W, O. Fujiwara, S. Watanabe, “Approximation of aging effect on dielectric tissue properties for SAR assessment of mobile telephones”, IEEE Transactions on Electromagnetic Compatibility, vol.48, no.2, pp.408-413, May.2006.

[41] Christ, A. and Kuster, N, “Differences in RF energy absorption in the heads of adults and children. Bioelectromagnetics”, 2005.

[42] Camelia Gabriel, “Compilation of the dielectric properties of body tissues at RF and microwave frequencies”, AFOSR/NL, Boiling AFB DC 20332-0001, 1995.

[43] Elio P., Jack W., Gail G.H., Per B., “Measurement of total body electrical conductivity: a new method for estimation of body composition.”, May,1983.

[44] Ernst, T., Kreis, R., & Ross, B. D., “Absolute Quantitation of Water and Metabolites in the Human Brain. I. Compartments and Water.”, Journal of Magnetic Resonance, Series B, 102(1), 1–8. doi:10.1006/jmrb.1993

[45] Celik, D. “Computation of the Cell Phone-Induced SAR Distribution in a 3 D Multi-Layered Model of the Human Head / Brain Using ANSYS,” 2013.

[46] Morimoto R., Laakso I., De S. V., Hirata A., “Relationship between peak spatial-averaged specific absorption rate and peak temperature elevation in human head in frequency range of 1-30 GHz,” Physics in medicine and biology, 61. 5406-5425,2016.

[47] Vladimir S, Dejanj, Dejan k, Vera M, Momir D,” Calculation of electromagnetic field from mobile phone induced in the pituitary gland of children head model”. Oct 2016.

[48] Bhargav, H. Srinivasan, T.Varambally, S., “Effect of Mobile Phone-Induced Electromagnetic Field on Brain Hemodynamics and Human Stem Cell Functioning: Possible Mechanistic Link to Cancer Risk and Early Diagnostic Value of Electron photonic Imaging”.Jan.2019.

[49] Yadolah F., Monireh M., “Comparison Nokia, Samsung and Sony mobile phones in the specific absorption rate of head induced to electric field”.2016.

[50] A.D. Usman., Wan Ahmad. W., Kadir. Z., Mokhtar. M., “Wireless Phones Electromagnetic Field Radiation Exposure Assessment”, American Journal of Engineering and Applied Sciences, Apr.2009.

[51] ICNIRP guidelines for limiting time-varying electric, magnetic and electromagnetic fields (up to 300 GHZ), health physics 74 (4):494-522; 1998

[52] Camelia G., and Sami G., “Compilation of the dielectric properties of body tissues at RF and Microwave frequencies”, King's College London, February 1996.